nature cell biology

Endocytosis of the seven-transmembrane RGS1 protein activates G-protein-coupled signalling in *Arabidopsis*

Daisuke Urano[1,4], Nguyen Phan[1,4], Janice C. Jones[2], Jing Yang[1], Jirong Huang[1], Jeffrey Grigston[1], J. Philip Taylor[1] and Alan M. Jones[1,3,5]

Signal transduction typically begins by ligand-dependent activation of a concomitant partner that is otherwise in its resting state. However, in cases where signal activation is constitutive by default, the mechanism of regulation is unknown. The *Arabidopsis thaliana* heterotrimeric Gα protein self-activates without accessory proteins, and is kept in its resting state by the negative regulator, AtRGS1 (regulator of G-protein signalling 1), which is the prototype of a seven-transmembrane receptor fused with an RGS domain. Endocytosis of AtRGS1 by ligand-dependent endocytosis physically uncouples the GTPase-accelerating activity of AtRGS1 from the Gα protein, permitting sustained activation. Phosphorylation of AtRGS1 by AtWNK8 kinase causes AtRGS1 endocytosis, required for both G-protein-mediated sugar signalling and cell proliferation. In animals, receptor endocytosis results in signal desensitization, whereas in plants, endocytosis results in signal activation. These findings reveal how different organisms rearrange a regulatory system to result in opposite outcomes using similar phosphorylation-dependent endocytosis mechanisms.

Many cells employ coordinated mechanisms to control the amplitude, duration and spatial distribution of G-protein-mediated responses to extracellular signals that activate seven-transmembrane (7TM) G-protein-coupled receptors. One such mechanism is 7TM receptor internalization, which physically removes the receptor from the cell surface to desensitize cells from continuous stimulation of the G-protein complex by the activated receptor[1,2]. Here we report identification of a previously unknown mechanism of signal control where internalization of a 7TM RGS protein leads to sustained signalling.

Recently, we discovered that the model plant organism *Arabidopsis thaliana* employs signal regulation mechanisms distinct from those identified in animals[3,4]. In contrast to animals, the *Arabidopsis* Gα protein self-activates without the aid of a receptor because its rate of guanine nucleotide exchange is about 100 times faster than its rate of GTP hydrolysis[3,4]. Consistent with this self-activating property, the *Arabidopsis* genome encodes no canonical 7TM, G-protein-coupled receptors[5,6] (GPCRs). However, the *Arabidopsis* genome encodes a 7TM domain fused to an RGS protein, AtRGS1, that stimulates the rate-limiting GTPase activity of the *Arabidopsis* Gα subunit, AtGPA1 (refs 3,7,8).

AtRGS1 and its cognate heterotrimeric G-protein complex are required for normal glucose sensing, cell proliferation, cell elongation and development[8–12]. Genetic evidence suggests that D-glucose or a sugar metabolite regulates AtRGS1 activity towards AtGPA1 (refs 3,8), although direct evidence for glucose binding to RGS1 is lacking and the molecular basis of how D-glucose and AtRGS1 control G protein signalling is not known.

Here we show that D-glucose causes AtRGS1 endocytosis. This sugar-dependent re-localization physically uncouples the inhibitory activity of AtRGS1 from the plant Gα protein, leaving the Gα protein constitutively active at the cell surface for sustained signalling. These results reveal how land plants employ RGS protein internalization to sense energy status and regulate growth and development. The presence of 7TM–RGS proteins in fungi and single-cell eukaryotes suggests that this mechanism is used in other organisms.

RESULTS

AtRGS1 internalizes in response to D-glucose

Mutations in *Arabidopsis* G proteins confer altered responsiveness to glucose[8,13,14]. As AtRGS1 contains a predicted 7TM domain reminiscent

[1]Department of Biology, University of North Carolina at Chapel Hill, Chapel Hill, North Carolina 27599, USA. [2]Department of Biochemistry and Biophysics, University of North Carolina at Chapel Hill, Chapel Hill, North Carolina 27599, USA. [3]Department of Pharmacology, University of North Carolina at Chapel Hill, Chapel Hill, North Carolina 27599, USA. [4]These authors contributed equally to this work.
[5]Correspondence should be addressed to A.M.J. (e-mail: alan_jones@unc.edu)

Received 1 December 2011; accepted 27 July 2012; published online 2 September 2012 ; DOI: 10.1038/ncb2568

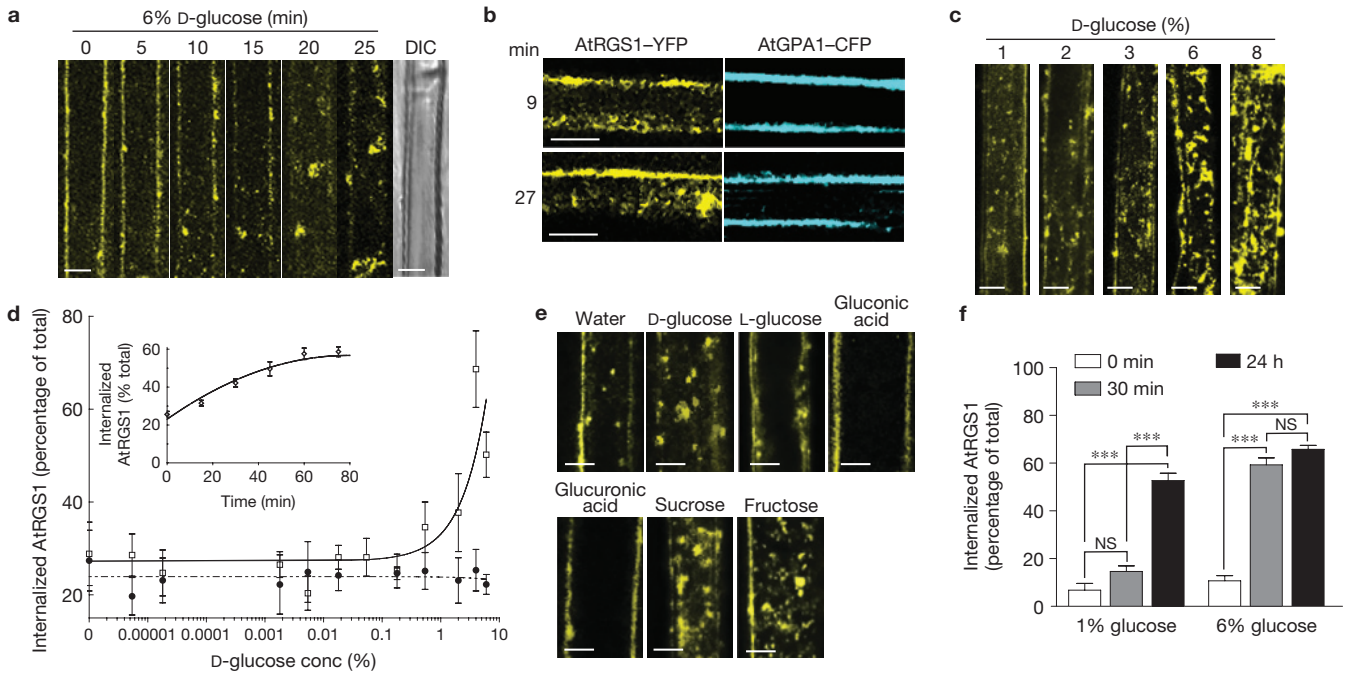

Figure 1 AtRGS1 internalizes in response to sugar. AtRGS1–YFP internalized by glucose. (**a**,**b**) Localization of AtRGS1–YFP (**a**) and AtGPA1–CFP (**b**) after treatment with 6% glucose in an *Arabidopsis* hypocotyl epidermal cell. Differential interference contrast (DIC) shows that 30 min treatment of glucose does not disrupt cell integrity (last in series, **a**). (**c**) Dose-dependent internalization of AtRGS1. *Arabidopsis* cells stably expressing AtRGS1–YFP imaged after treatment with varying concentrations of glucose for 30 min. (**d**) Quantification of dosage response of AtRGS1 (open squares) and AtRGS1^{E320K} mutant (GAP dead; filled circles) with increasing glucose concentrations. At the 30 min time point, YFP fluorescence intensity was measured by subtracting internalized RGS1–YFP fluorescence signal from the total cell fluorescence signal. A point mutation that inhibits AtRGS1 interaction with AtGPA1, AtRGS1^{E320K}, disrupts AtRGS1–YFP internalization. Error bars, s.e.m., $n = 5$. Inset: Quantification of the glucose dosage response of AtRGS1–YFP internalization imaged at 30 min post-glucose treatment. Error bars, s.e.m., $n = 5$. (**e**) Sugar specificity of AtRGS1 internalization. Several sugar and sugar analogues (6% of each) were applied to seedlings expressing AtRGS1–YFP for 30 min before imaging as described in Methods. (**f**) RGS1–YFP reciprocity of time and dose dependence. AtRGS1 seedlings stably expressing AtRGS1–YFP were treated without or with 1% or 6% D-glucose. After 30 min or 24 h treatment, internalized AtRGS1 was quantified. Error bars, s.e.m., $n = 5$. NS, not significant ($P > 0.05$); ***, highly significantly different ($P < 0.001$). Scale bars, 10 μm. Quantification of fluorescence intensity is described in Methods.

of GPCRs, localizes to the cell surface and interacts with the plant Gα protein in a glucose-dependent manner, AtRGS1 was proposed to be a glucose receptor or co-receptor in G-protein-mediated glucose sensing[3,8,13,15,16].

In animals, ligand-induced 7TM receptor endocytosis desensitizes cells to the ligand by reducing the amount of receptor at the cell surface[1]. To determine the effect of the candidate ligand on AtRGS1 internalization, epidermal cells expressing AtRGS1–YFP were treated with several concentrations of D-glucose, and the subcellular localization of AtRGS1 was captured over time (Fig. 1 and Supplementary Fig. S1a). The maximum steady-state level of internalized AtRGS1 varied between 60% and 90%, depending on expression levels, and was reached within 60 min. Three-dimensional reconstruction revealed that the observed change in AtRGS1 was due to internalization as opposed to clustering on the plasma membrane (Supplementary Movie S1). AtRGS1 internalization showed glucose dose dependence (Fig. 1c,d) and structural stereo-specificity in that D- but not L-glucose caused internalization (Fig. 1e). Likewise, two similar structures, gluconic and glucuronic acids (Fig. 1e), did not affect AtRGS1 localization. Three analogous sugars, mannose, fructose and sucrose, each able to yield glucose through metabolism[17–19], induced AtRGS1 internalization (Fig. 1e). General reciprocity was observed between the dose dependence and time dependence of AtRGS1 internalization; 1% D-glucose induced internalization (Fig. 1c,d), but required 24 h to reach the maximum achieved by the acute dose of 6% in 30 min (Fig. 1f).

To eliminate the possibility that glucose caused a general and nonspecific sweep of membrane proteins from the plasma membrane, we tested a 7TM domain protein, AtMLO6 (refs 20,21; Supplementary Fig. S1b, bottom pair), and showed that this plasma membrane 7TM protein does not internalize with glucose. These results show that the effect of D-glucose on AtRGS1 internalization is specific, as well as time and dose dependent.

A critical observation was that whereas AtRGS1–YFP internalized by glucose, the cognate Gα, CFP–AtGPA1 co-expressed in the same cell, did not (Fig. 1b). No internalization of CFP–AtGPA1, was observed at any tested glucose dose including the 6% acute treatments even when monitored over extended observation times using both stably (Fig. 1b) or transiently transformed cells (Supplementary Fig. S1b, centre pair). Taken with the AtRGS1 data above, we conclude that glucose causes physical separation of the plant Gα subunit from AtRGS1.

Animal GPCRs are internalized through the endosomal pathway[22–24]. To determine the localization of AtRGS1 after internalization, we measured AtRGS1 co-localization with various compartmental

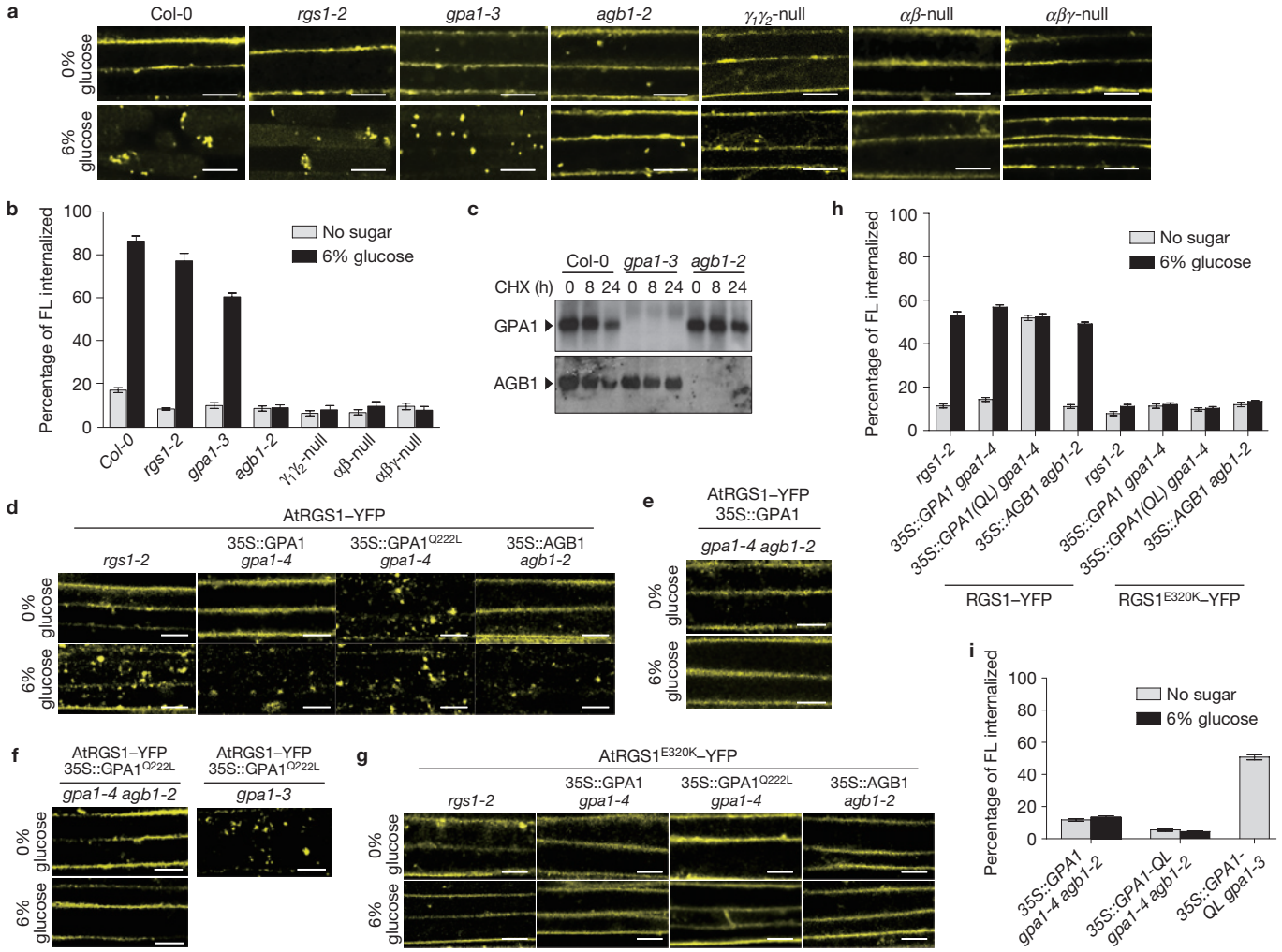

Figure 2 AGB1 is essential for AtRGS1 internalization. (**a**) AtRGS1–YFP was transiently expressed in an informative set of G-protein mutants and these were treated with 6% glucose. Internalization of AtRGS1–YFP was imaged in Col-0, *rgs1-2*, *gpa1-3*, *agb1-2*, *agg1-2 agg2-1* double null mutants ($\gamma_1\gamma_2$-null), *gpa1-4 agb1-2* double null mutants ($\alpha\beta$-null) and *gpa1-4 agb1-2 agg1-2 agg2-1* quadruple null mutants ($\alpha\beta\gamma$-null) without and with 6% glucose. (**b**) Quantification of the percentage of AtRGS1–YFP fluorescence (FL) signal internalized in epidermal cells before and after glucose stimulation. Error bars, s.e.m., $n = 5$. (**c**) Seedlings of Col-0, *gpa1-3* and *agb1-2* were treated with 200 mM cycloheximide (CHX). Relative steady-state levels of AtGPA1 and AGB1 protein in the seedling were analysed by immunoblot analysis with anti-AtGPA1 and anti-AGB1 antisera. (**d**) AtRGS1–YFP was transiently expressed in *rgs1-2* null mutants, 35S::AtGPA1, 35S:: AtGPA1^{Q222L} (active mutant) or 35S::AGB1 lines and treated with 6% glucose. 35S:: represents a constitutive promoter from the cauliflower mosaic virus used for ectopic overexpression. (**e**) AtRGS1–YFP and 35S::AtGPA1 were transiently expressed in a *gpa1-4 agb1-2* double mutant and treated with 6% glucose. (**f**) Both AtRGS1–YFP and 35S:: AtGPA1^{Q222L} were transiently expressed in the *gpa1-4 agb1-2* double mutant and treated with 6% glucose (left panels). AtRGS1–YFP and 35S:: AtGPA1^{Q222L} were also transiently expressed in the *gpa1-3* mutant (right panel). (**g**) AtRGS1^{E320K}–YFP was transiently expressed in *rgs1-2* null mutants, 35S::AtGPA1, 35S:: AtGPA1^{Q222L} (active mutant) or 35S::AGB1 lines then treated with 6% glucose before imaging. (**h**) Quantification of the percentage of AtRGS1–YFP and AtRGS1^{E320K}–YFP fluorescence signal internalized in epidermal cells before and after 6% glucose stimulation. Error bars, s.e.m., $n = 5$. The genetic background is indicated: *rgs1-2*, ectopic expression of AtGPA1 (35S-GPA1 in *gpa1-4* null background), ectopic expression of constitutively active AtGPA1 (35S:: GPA1^{Q222L} in *gpa1-4* null background), and ectopic expression of AGB1 (35S::AGB1 in *agb1-2* null background). (**i**) Quantification of the percentage of AtRGS1–YFP fluorescence signal in epidermal cells transiently expressing the AtGPA1 in the *gpa1/agb1* double mutant (35S::AtGPA1 in *gpa1-4 agb1-2* null background), constitutively active AtGPA1 (35S::GPA1-QL) in the *gpa1/agb1* double mutant), and 35S::GPA1-QL in the *gpa1-3* mutant). Error, s.e.m., $n = 5$. Scale bars, 10 μm. GPA1-QL represents GPA1^{Q222L}. Quantification of fluorescence signal is described in Methods. Uncropped images of blots are shown in Supplementary Fig. S8.

markers in epidermal pavement cells. AtRGS1 co-trafficked with the endosomal dye FM4-64 (Supplementary Fig. S2a), endosomal markers that reside in the early to late endosomes (Supplementary Fig. S2). Co-expression of AtRGS1–YFP with RFP-tagged compartment markers was also performed using tobacco cells because their larger size provides the required spatial resolution for co-localization (Supplementary Fig. S2b). Of particular interest was the observed 100% co-localization of AtRGS1 with SYP23 (Supplementary Fig. S2b), a late endosomal syntaxin because AtRGS1 and SYP23 are known to physically interact[25]. AtRGS1–YFP did not co-localize with the mitochondrial-RFP marker[26] (Mt-rk; Supplementary Fig. S2b). These results indicate that AtRGS1–YFP internalization occurs through the endocytic pathway and hereafter we refer to the observation of AtRGS1 internalization as endocytosis.

Free Gβ, AGB1, is essential, but not sufficient, for AtRGS1 endocytosis

The amount of D-glucose-induced endocytosis of AtRGS1–YFP was reduced by 40% in the absence of the Gα subunit AtGPA1 (*gpa1-3*), and completely abrogated in the absence of the Gβ subunit AGB1 (Fig. 2a,b). Loss of AtGPA1 or AGB1 individually did not markedly affect the steady-state levels of the respective protein-binding partner (Fig. 2c), suggesting that both G-protein components, particularly the Gβ subunit, directly mediate glucose-stimulated AtRGS1 endocytosis.

The complete loss of AtRGS1 trafficking in the *agb1*-2 background was genetically complemented by ectopic expression of AGB1 (Fig. 2d,h). Ectopic overexpression of wild-type AtGPA1 did not significantly affect AtRGS1 trafficking (Fig. 2d). However, overexpression of the constitutively active AtGPA1 mutant (GTPase-deficient $AtGPA1^{Q222L}$) in the absence of the wild-type Gα subunit triggered AtRGS1 endocytosis without glucose (Fig. 2d,h,i). This induction by $AtGPA1^{Q222L}$ of AtRGS1 endocytosis required AGB1 (Fig. 2e,f). Taken together, these results indicate that the Gβγ dimer is required for AtRGS1 endocytosis induced by D-glucose and that the activated Gα subunit plays a role in AtRGS1 endocytosis. Although these results suggest that the freed Gβ subunit is necessary, its release from the complex alone, an expectation for the Gα null mutants, is insufficient for AtRGS1 endocytosis.

Physical coupling of AtRGS1 and AtGPA1 is essential for AtRGS1 endocytosis

A charge reversal at Glu 320 of AtRGS1 uncouples the interaction between AtRGS1 and AtGPA1, and therefore abrogates the acceleration of GTP hydrolysis activity[3]. To determine whether AtRGS1 interaction with AtGPA1 is required for AtRGS1 endocytosis, we measured glucose-induced internalization of the $AtRGS1^{E320K}$ mutant protein. We found that $AtRGS1^{E320K}$–YFP did not internalize under conditions that promoted endocytosis of the wild-type protein (Figs 1d, 2d versus 2g, and 2h). To distinguish between a loss of interaction or failure to accelerate GTP hydrolysis, we combined the $AtGPA1^{Q222L}$ mutation with the $AtRGS1^{E320K}$ mutation. Although constitutively active $AtGPA1^{Q222L}$ caused glucose-independent internalization of wild-type AtRGS1, $AtGPA1^{Q222L}$ failed to trigger $AtRGS1^{E320K}$ internalization under any condition (Fig. 2d,g). These results indicate that a physical interaction between AtGPA1 and AtRGS1 is required for AtRGS1 endocytosis, but AtGPA1 cycling between inactive and active states is dispensable for initiating the AtRGS1 internalization process. One interpretation is that without AtRGS1 interaction with AtGPA1, the heterotrimer forms, thus sequestering AGB1, shown to be essential for AtRGS1 endocytosis (Fig. 2a,b).

AtWNK8 is an AtRGS1 kinase

On sustained ligand occupancy, mammalian GPCRs are phosphorylated by G-protein receptor kinases (GRKs). This phosphorylation event is critical for assembly of the trafficking complex and concomitant receptor endocytosis[1,27]. Thus, we reasoned that AtRGS1 phosphorylation is required for AtRGS1 endocytosis. When calyculin A, a Ser/Thr phosphatase inhibitor[28], was applied to *Arabidopsis* seedlings, a band shift for AtRGS1, but not AtGPA1, was observed using SDS–polyacrylamide gel electrophoresis (SDS–PAGE; Fig. 3a), suggesting the phosphorylation of AtRGS1 *in vivo*. Likewise, calyculin A accelerated receptor endocytosis even in the absence of glucose, suggesting tonic cycling (Fig. 3b; $P < 0.01$). In contrast, the mobilities of AtRGS1 and AtGPA1 were not changed by the tyrosine phosphatase inhibitor sodium orthovanadate (Fig. 3a). These data suggest that AtRGS1 phosphorylation on Ser/Thr residues promotes endocytosis.

AtRGS1 has many di-serines at its carboxy terminus, analogous to the sequence found in vertebrate GPCRs that are phosphorylated, a requisite for endocytosis in response to their ligands[1,27]. Although the *Arabidopsis* genome encodes tenfold more kinases than the human genome[29], none of these plant kinases has the GRK architecture typified by an amino-terminal RGS-homology domain[30]. Therefore, we searched *ab initio* for candidate AtRGS1 kinases among candidate AtRGS1-interacting proteins that were identified from yeast complementation screens[25,31]. We found several AtRGS1-interacting kinases (Supplementary Fig. S3a) and confirmed *in vivo* interactions using bimolecular fluorescence complementation (BiFC, Supplementary Fig. S3b). Although all four kinases assigned to the G-protein interactome interacted with AtRGS1, only AtWNK8, among these, phosphorylated a recombinant AtRGS1 substrate (RGS box + Ct (amino acids 284–459)) under these *in vitro* conditions (Supplementary Fig. S3a).

AtWNK8 is one of 11 WNK (WITH NO LYSINE) family Ser/Thr kinases in *Arabidopsis* (Fig. 3c). Although this kinase family has the catalytic lysine at the expected location in the catalytic centre, it is at an unusual position in the linear sequences[32]. To address AtRGS1 specificity for WNK family members, we measured interactions using yeast two-hybrid (Supplementary Fig. S3c), BiFC (Supplementary Fig. S3b) and *in vitro* co-precipitation assays (Fig. 3d). We included AtWNK1, the most divergent from AtWNK8, and AtWNK10, the most similar to AtWNK8 in sequence (Fig. 3c). AtRGS1 interacted with all three representative WNK family kinases in all three assays, but AtRGS1 was phosphorylated by AtWNK8 the most under these experimental conditions (Fig. 3e,f; compare AtRGS1 phosphorylation with the respective AtWNK autophosphorylation band). Although AtWNK1 and AtWNK10 have lower specific activities, these kinases are clearly able to phosphorylate AtRGS1 under these *in vitro* conditions.

Having identified kinases that phosphorylate AtRGS1 *in vitro*, we next determined how these kinases affected AtRGS1 endocytosis *in vivo* using genetic ablation (alleles shown in Supplementary Fig. S3e,f). Towards this end, we measured AtRGS1 trafficking in the absence of the selected WNK kinases with and without 6% D-glucose (Fig. 3g). AtRGS1 was internalized in Col-0 and *wnk1* cells, but not in the absence of AtWNK8 (*wnk8-1* and *wnk8-2* alleles) or AtWNK10 (*wnk10-2*) or both AtWNK8 and AtWNK10 (*wnk8-1/wnk10-1*). These results shown in Fig. 3g indicate that AtWNK8 and AtWNK10, but not WNK1, are AtRGS1 kinases that drive AtRGS1 endocytosis.

AtRGS1 endocytosis requires C-terminal phosphorylation

AtRGS1 has 11 serines within its 50 most C-terminal residues that are candidate phosphorylation sites. Our *in vitro* phosphorylation of RGS box + Ct showed ~2 moles $^{32}PO_4$ incorporated per mole of substrate (Supplementary Fig. S4a). Liquid chromatography–tandem mass spectrometry analysis of recombinant RGS box + Ct phosphorylated by AtWNK8 identified two phosphorylation sites: Ser 428 and Ser 435 or Ser 436 (Fig. 4a,b and Supplementary Fig. S4c,d) in the AtRGS1 C terminus. To validate the tandem MS results, we determined whether

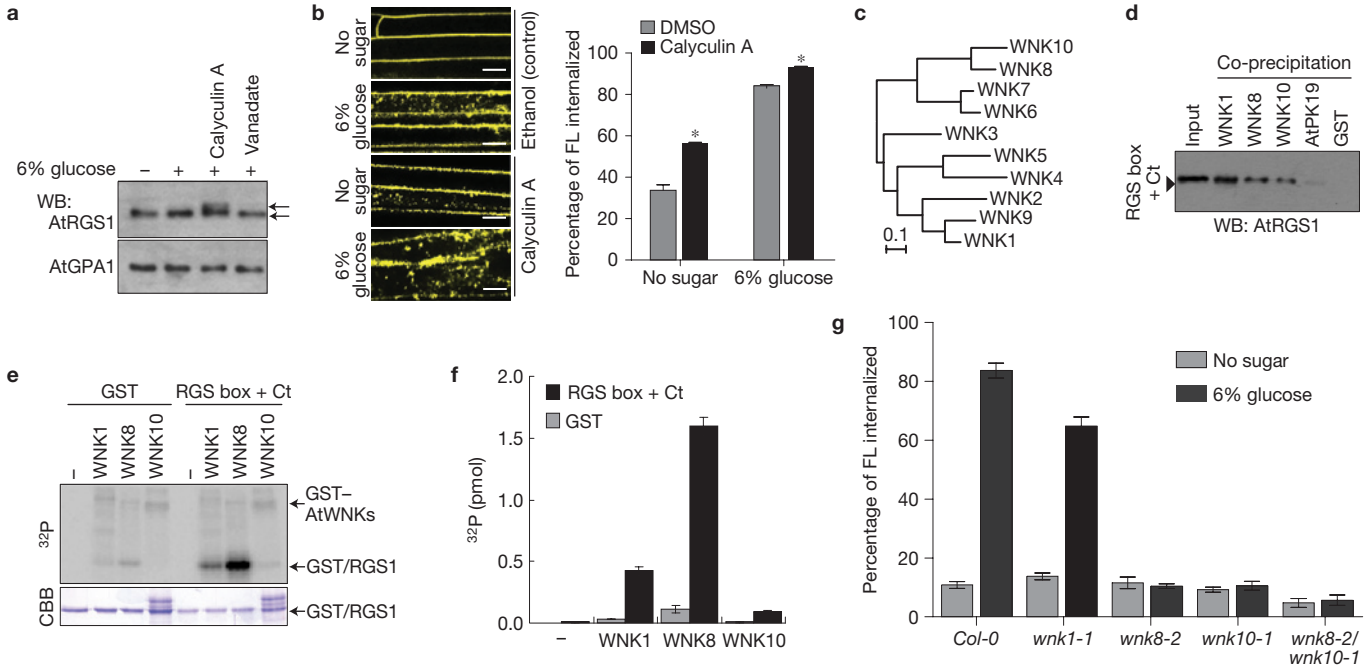

Figure 3 *In vivo* and *in vitro* function of AtWNK8. (**a**) *In vivo* phosphorylation of AtRGS1. Seedlings expressing AtRGS1–TAP were pretreated with 100 nM calyculin A and 10 mM sodium orthovanadate for 3 h followed by 6% D-glucose stimulation for 90 min. AtRGS1–TAP or AtGPA1 in seedling lysates was separated on a 12.5% Anderson's gel and detected by immunoblot with peroxidase anti-peroxidase or anti-AtGPA1 antibody. (**b**) Four-day-old AtRGS1–YFP-expressing seedlings were treated with phosphatase inhibitor, calyculin A, for 2 h followed by 6% glucose treatment or not for 1 h before imaging epidermal cells. Scale bars, 10 μm. Error, s.e.m., $n = 5$. (**c**) Phylogenetic tree of the AtWNK family kinases. Full-length amino-acid sequences were aligned with CLUSTAL W implemented in CLC Genomics Workbench using the following settings; Gap open penalty, 10; Gap extension penalty 1. The neighbour joining tree (1,000 bootstrap replicate) was created with the aligned sequences. (**d**) *In vitro* binding between AtRGS1 and AtWNKs. Recombinant RGS box + Ct was tested for interaction with GST (negative control) or GST–AtWNKs using glutathione–Sepharose, and detected by immunoblot analysis using an anti-AtRGS1 antibody. (**e**) *In vitro* phosphorylation of AtRGS1 by AtWNK kinases. Recombinant GST or His–RGS box + Ct was incubated with GST–AtWNKs in reaction buffer containing [γ-^{32}P]ATP. Proteins were separated by SDS–PAGE. Coomassie brilliant blue (CBB) was used to stain either the GST or RGS1 proteins. (**f**) Radioactivity incorporated into the GST or RGS1 bands. Coomassie brilliant blue (CBB) staining of either the GST or RGS1 proteins. Phosphorylation levels of three independent experiments were quantified in **e**. Error bars, s.e.m. (**g**) Quantification of sugar-induced AtRGS1 internalization in AtWNK-null mutants. Seedlings of Col-0, *wnk1-1*, *wnk8-1*, *wnk8-2* or *wnk10-2* transiently expressing AtRGS1–YFP were treated with 6% D-glucose for 30 min. WNK# denotes AtWNK members in **c**–**f**. Error bars, s.e.m., $n = 5$. Quantification of fluorescence intensity is described in Methods. Uncropped images of gels/blots are shown in Supplementary Fig. S8.

AtWNK8 phosphorylates *in vitro* an AtRGS1 substrate lacking the C-terminal domain (AtRGS1-RGS box; amino acids 284–416) and the isolated C-terminal domain (AtRGS1-Ct; amino acids 400–459). AtWNK8 preferentially phosphorylated AtRGS1 substrates that contained both the RGS and the C-terminal domains (Fig. 4d,e) and this result correlated with stronger interactions in co-precipitation assays using purified proteins (Fig. 4c). In BiFC experiments, cYFP–AtWNK8 specifically interacted with AtRGS1–nYFP but not with the mutant lacking the C-terminal domain (ΔCt; amino acids 1–416, Fig. 4b and Supplementary Fig. S4e), although both AtRGS1–cYFP and the ΔCt mutant interacted with cYFP–AtGPA1 as a positive control. These results indicate that the C-terminal domain on AtRGS1 is necessary for phosphorylation and interaction with AtWNK8 and that the RGS box plays a structural role in these processes. As our MS analyses failed to identify phosphopeptides from the extreme C terminus of AtRGS1 (non-highlighted sequence in Supplementary Fig. S4b), we do not exclude other phosphorylation sites in this region. However, as we showed that the specific activity is 2 moles of phosphate per mole of AtRGS1 C-terminal fragment (Supplementary Fig. S4a), these other phosphorylation sites would be mutually exclusive to the ones identified.

We generated phospho-specific AtRGS1 antibodies for immunoblot analysis. In *Arabidopsis* seedling lysates, AtRGS1–TAP (tandem affinity protein tagged) was phosphorylated on D-glucose treatment (Fig. 4f). The phosphatase inhibitor calyculin A increased AtRGS1 phosphorylation, even without D-glucose (Fig. 4f,g), suggesting that AtRGS1 undergoes steady-state phosphorylation and dephosphorylation in plant cells.

As phosphorylation of animal GPCRs is critical for their endocytosis, we engineered a C-terminal truncation mutant (AtRGS1$^{\Delta CtSA}$) and a full-length AtRGS1^{3SA} mutant (S428A/S435A/S436A) in which three phosphorylation sites identified were mutated to alanine residues (Fig. 4b), and assayed for D-glucose-dependent endocytosis. Whereas the wild-type AtRGS1–YFP was localized to the plasma membrane and endocytosed on D-glucose treatment, the AtRGS1^{3SA} mutant (Fig. 4h,i) or AtRGS1$^{\Delta CtSA}$ (Fig. 4j) remained at the plasma membrane with D-glucose in both stable and transient expression assays. Furthermore, whereas steady-state levels of phosphorylated full-length AtRGS1 increased with phosphatase inhibition by calyculin A, no equivalent change was observed for the AtRGS1$^{\Delta CtSA}$ mutant (Fig. 4g). These results indicate that the C terminus on AtRGS1 is the

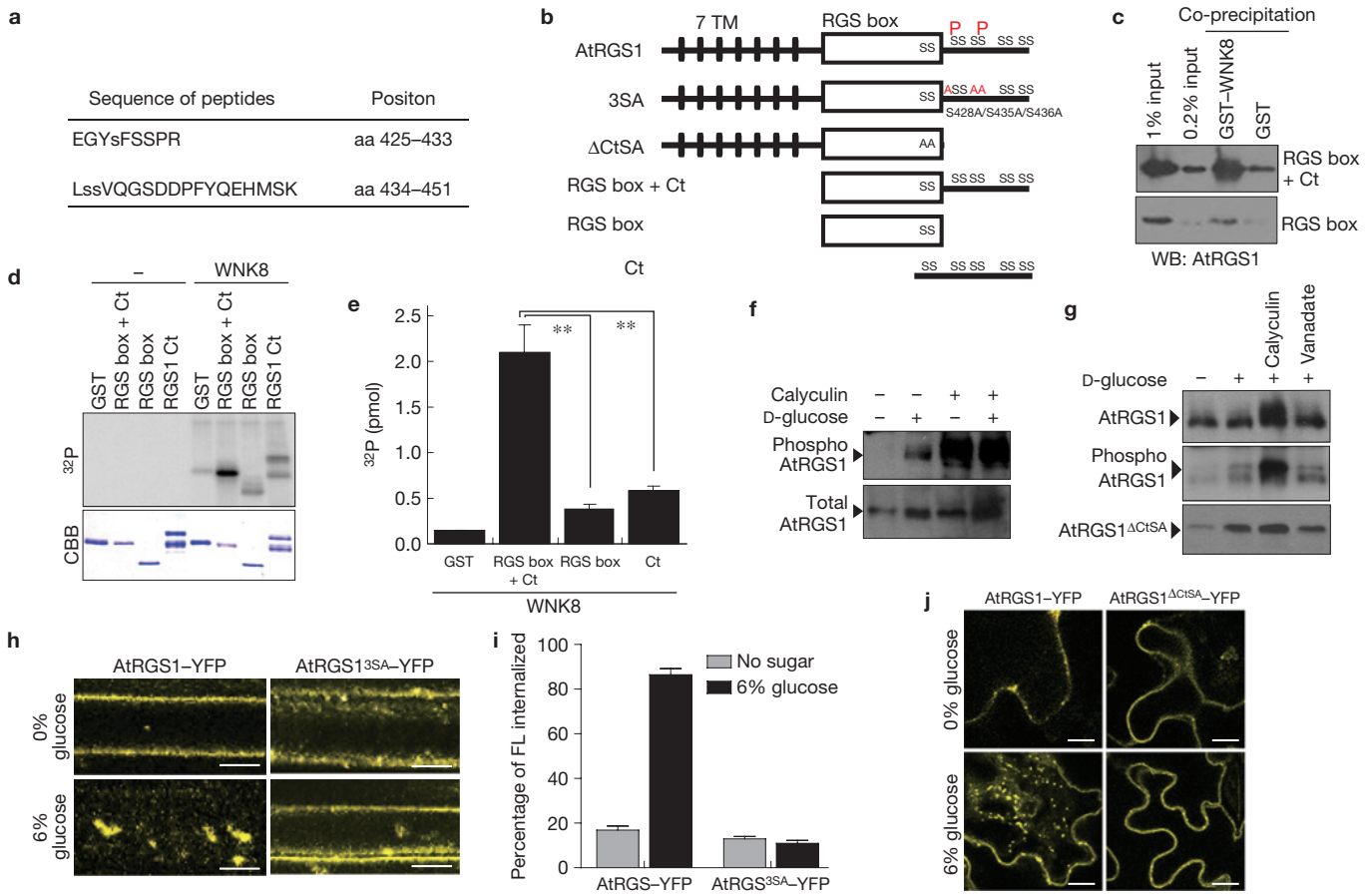

Figure 4 Phosphorylation and function of the C terminus of AtRGS1. (**a**) Phosphorylated peptides of AtRGS1 isolated and identified by tandem mass spectrometry. Recombinant RGS box + Ct was phosphorylated by AtWNK8, trypsinized and subjected to liquid chromatography–tandem mass spectrometry as described in the Methods. (**b**) Schematic model of AtRGS1 mutants. Transmembrane (TM) regions are shown as black lines, AtRGS1 box as a white rectangle and the identified phosphorylation sites are denoted P. (**c**) *In vitro* binding between AtRGS1 truncated mutants and AtWNK8. Recombinant RGS box + Ct or RGS box of AtRGS1 was tested for interaction with GST (negative control) or GST–AtWNK8. Inputs and precipitated proteins were analysed by immunoblot analysis using an anti-AtRGS1 antibody. (**d**) *In vitro* phosphorylation of AtRGS1 by AtWNK8. Recombinant His-tagged RGS box + Ct, RGS box or GST–AtRGS1-Ct plus [γ-^{32}P]ATP were incubated with (WNK8) or without (-) GST–AtWNK8. Radiolabelled (^{32}P) proteins were separated by SDS–PAGE and detected as described in the Methods. (**e**) The levels of phosphorylation were quantified. Error bars, s.e.m., $n = 4$. **, $P < 0.01$. (**f**) *In vivo* phosphorylation of AtRGS1. Seedlings expressing AtRGS1–TAP were pretreated with 100 nM calyculin A for 3 h followed by 6% D-glucose for 90 min. Phosphorylation of AtRGS1 was detected by immunoblot analysis using an anti-phospho-AtRGS1 antibody or peroxidase anti-peroxidase (total RGS1). (**g**) *In vivo* phosphorylation of AtRGS1 or the ΔCtSA mutant. TAP-tagged AtRGS1 or AtRGS1$^{\Delta CtSA}$ seedlings were pretreated with 100 nM calyculin A or 10 mM sodium orthovanadate for 3 h followed by 6% D-glucose stimulation for 90 min. AtRGS1 or AtRGS1$^{\Delta CtSA}$ lysate was separated on a 12.5% Anderson's gel and subjected to immunoblot analysis using anti-phospho-AtRGS1 antibody or peroxidase anti-peroxidase (total RGS1, RGS1$^{\Delta CtSA}$). (**h**) Internalization of AtRGS1–YFP and AtRGS1-3xSA–YFP. AtRGS1–YFP and AtRGS1-3xSA–YFP were transiently expressed, followed by 30 min treatment in 6% glucose before imaging. Scale bars, 10 μm. (**i**) Quantification of AtRGS1–YFP and AtRGS1-3xSA–YFP fluorescence internalization. Error bars, s.e.m., $n = 5$. (**j**), Internalization of the full-length and C-terminal truncated mutant of AtRGS1. AtRGS1–YFP or AtRGS1$^{\Delta CtSA}$ was expressed in tobacco leaves and treated with 6% D-glucose for 30 min. WNK8 denotes AtWNK8. Scale bars, 20 μm. Quantification of fluorescence signal is described in Methods. Uncropped images of blots/gels are shown in Supplementary Fig. S8.

only phosphorylation region and that C-terminal phosphorylation is required for AtRGS1 endocytosis.

Gβγ subunit interacts with AtWNK8 on the plasma membrane

AtWNK8 is known to interact with the β-propeller protein AtRACK1 (ref. 25), which has a similar structure to the Gβ protein AGB1 (ref. 33). Thus, we reasoned that AtWNK8 directly interacted with AGB1 as well. We found, using purified components, that AtWNK8 directly interacted with AGB1/AGG1 in co-precipitation experiments, but AtWNK8 did not interact with AtGPA1 (Fig. 5a,b). Using BiFC analysis, AGB1/AGG1 strongly interacted with AtWNK8 at the plasma membrane in both stable and transient assays (Fig. 5c and Supplementary Fig. S5), although most WNK8 was cytoplasmic (Fig. 5d). This indicates that the rate-limiting factor is the level of available Gβγ dimer at the plasma membrane.

Fluorescence resonance energy transfer (FRET) analysis showed that AtWNK8 association with AtRGS1 increased on treatment with 6% D-glucose (Fig. 5d). Within minutes of stimulation, the AtWNK8 associated with AtRGS1 at the plasma membrane (5 min; $P < 0.05$) followed by the endosomes (30 min.; $P < 0.05$). The FRET results suggest that the association of AtWNK8 and AtRGS1 at the plasma membrane is triggered by induction of glucose (Fig. 5d, 5 min. time

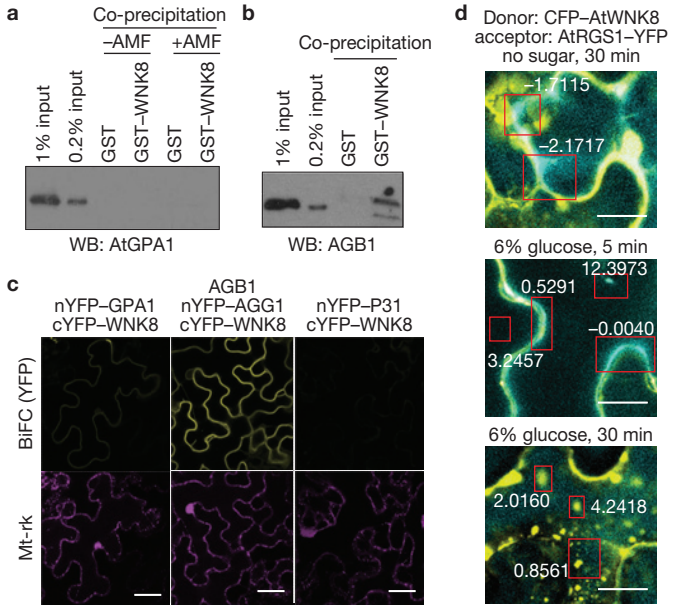

Figure 5 AtWNK8 physically interacts with the G-protein βγ subunit. (**a**,**b**) *In vitro* binding between AtWNK8 and heterotrimeric G protein. Inactive, GDP-bound AtGPA1, AtGPA1 activated by aluminium tetrafluoride (AMF: 50 μM GDP, 30 μM $AlCl_3$, 10 mM $MgCl_2$ and 5 mM NaF) or AGB1/AGG1 was co-precipitated with GST or GST–AtWNK8. Proteins were subjected to immunoblot analysis with anti-AtGPA1 or anti-AGB1 antisera. The two different amounts of input protein (0.2% or 1% of total) were loaded as a reference. (**c**) *In vivo* binding between AtWNK8 and heterotrimeric G protein. nYFP-tagged AtGPA1, AGG1 with AGB1, or P31 was co-transformed with cYFP-tagged AtWNK8 and mitochondrial marker (Mt-rk, transformation control) into tobacco leaves. Fluorescence complementation of split YFP and expression of RFP were observed by confocal fluorescence microscopy. Scale bars, 50 μm. (**d**) CFP–AtWNK8 associates with AtRGS1–YFP. Acceptor photobleaching of CFP–AtWNK8 and AtRGS1–YFP transiently expressed in tobacco in no sugar and 6% D-glucose for the indicated times. Bleached zones are in outlined in red and numbers denote the net FRET value. WNK8 denotes AtWNK8. The method for determining the FRET efficiency indicated by the respective outlines is described in Methods. Scale bars, 20 μm. Uncropped images of blots are shown in Supplementary Fig. S8.

point). The interaction continued with trafficking into endocytic compartments (Fig. 5d, 30 min time point).

AtWNK8/10 is required for activation of G-protein signalling

Glucose/fructose signalling through AtRGS1 is known to activate transcription of the *TBL26* gene[16] (At4G01080) and therefore glucose-induced *TBL26* expression is used as a reporter of AtRGS1-dependent sugar signalling. We found that *TBL26* expression in cells lacking *AtRGS1* or both *AtWNK8* and *AtWNK10* was at the basal level, only 20% of the expression detected in wild-type cells treated with 6% D-glucose (Fig. 6a). These results were consistent with our earlier finding that AtRGS1 is endocytosed in 6% D-glucose, and minimally or not at all at a lower concentration and a shorter duration of D-glucose treatment (Fig. 1). In the *rgs1-2* or *wnk8-2/wnk10-1* double-mutant cells, acute D-glucose treatment failed to stimulate *TBL26* expression at the wild-type level (Fig. 6a). Loss of WNK8 attenuated *TBL26* expression but loss of both WNK8 and 10 completely abrogated sugar signalling as reported by *TBL26* expression (Fig. 6a,b). Sugar-stimulated AtRGS1 endocytosis correlated with *TBL26* expression.

Previously, we identified a subset of genes that were induced by D-glucose in an AtRGS1-independent manner[16]. To determine the role of *AtWNK8* in expression of these other genes, we quantified their induction following a brief acute treatment with D-glucose. We found that induction of AtRGS1-dependent genes (*TBL26* and three Jacalin-like) were attenuated in *rgs1-2*, *gpa1*-4, *agb1*-2, *wnk8*-2 or *wnk10*-1 (Supplementary Fig. S6a). In contrast, *AtRGS1*-independent genes (At4G23600 and At5G48850) were similarly induced in all genotypes (Supplementary Fig. S6a). Likewise, the time course of D-glucose stimulation and reset timing after starvation was unaffected in *wnk8* null mutants (Fig. 6b and Supplementary Fig. S6b). Together, these results suggest that sugar signals are mediated by several different mechanisms, and AtWNK8 and AtWNK10 influence only the AtRGS1-dependent sugar signals. Moreover, these results suggest that AtWNK-mediated endocytosis of AtRGS1 is critical for activating G-protein-mediated sugar signalling.

AtRGS1 endocytosis activates cell division

G-protein signalling is involved in cell proliferation and elongation in *Arabidopsis* seedlings[9,10,13]. After 2 days of etiolated growth, *gpa1* or *agb1* seedlings have shorter hypocotyls than wild-type seedlings because of a reduction in cell proliferation[9,10]. On the other hand, *rgs1* plants and plants that express the constitutively active Gα, $AtGPA1^{Q222L}$, have longer hypocotyls[8]. A visual sugar phenotype of the G mutants is growth arrest and this is also a cell division phenomenon. We used the standard green seedling assay in conjunction with our sugar signalling assay[16] to illustrate the role of the WNK kinases. Figure 6a shows that over a range of glucose concentrations, sugar signalling is greatly attenuated in the *rgs1* single and *wnk8-2/10-1* double mutants (combination of a different set of *wnk8* and *wnk10* alleles gave the same results). Loss of WNK8 alone slightly reduces signalling over time when compared with wild type seedlings (Fig. 6b). Sugar signalling as reported by *TBL26* gene expression correlates with the growth behaviour on treatment with the acute level of D-glucose. Growth arrest on 6% glucose was more than 60% for wild-type seedlings yet only 15% for the *wnk8-2/10-1* double-mutant and 40% for the *wnk8-2* single-mutant seedlings (Fig. 6c). This was observed over a range of glucose concentrations (Fig. 6d). Consistent with the loss-of-function mutations, ectopic overexpression of either *WNK8* or *AtRGS1* confers the opposite effect (Fig. 6c versus d for WNK8 versus e for AtRGS1). The increased sensitivity to glucose conferred by AtRGS1 expression requires the C terminus and/or the serines targeted for phosphorylation by WNK8 (Fig. 6e). The role of glucose-induced AtRGS1 endocytosis fits the context of sugar-induced growth arrest and also suggests that sugar signalling for this growth behaviour originates, at least in part, at the endosome.

DISCUSSION

Signalling through the heterotrimeric G-protein complex is one mechanism by which plants sense sugar levels and regulate cell proliferation and cell elongation accordingly[3,8–11,13,15,16]. Unlike in humans, where the serum glucose levels are held nearly constant by a feedback mechanism involving glucose uptake and metabolism, both the apoplastic and symplastic glucose levels in plants swing over four orders of magnitude[34]. Diurnal changes in the rate of glucose production from photosynthesis account for most of this variation in glucose concentration, but also important are long-term

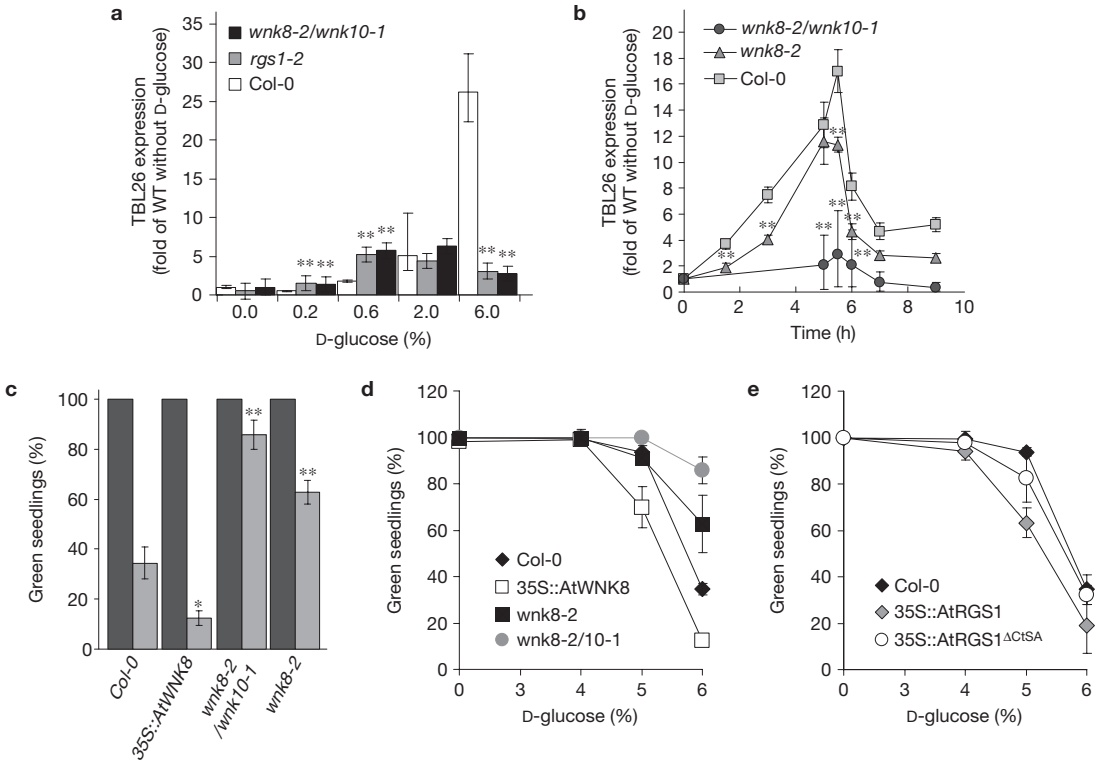

Figure 6 *wnk8* mutant expression and phenotypes. (**a**) Glucose signalling as reported by gene expression analysis in *wnk* mutants. Dose-dependent *TBL26* expression in Col-0, *rgs1-2* or *wnk8-2/wnk10-1*. Seven-day-old seedlings were starved for 2 days and then treated with various concentration of D-glucose for 3 h. *TBL26* transcript levels were normalized with that of Col-0 without D-glucose stimulation. Data show mean ± s.d. ($n = 3$) from a representative experiment. (**b**) Time course of *TBL26* expression and the reset timing. Seedlings were starved for 2 days and stimulated at time 0 with 6% D-glucose for 5 h then moved 1/2 × MS media lacking sugars (hour 5 to 9). *TBL26* expressions at each time period were normalized with the expression without D-glucose stimulation. Data show mean ± s.d. ($n = 3$) from a representative experiment. (**c**–**e**) Physiological sugar-related phenotype of *wnk and rgs1* mutants. Vernalized seeds of wild-type Col-0 or the indicated mutants were grown on 1/2 × MS plates containing 0%, 3%, 4%, 5% and 6% D-glucose at 23 °C under continuous light (50 μmol s^{-1} m^{-2}) for 10 days. The average number of seedlings having green cotyledons was determined and presented with s.e.m. The histogram in **c** provides the average plus s.e.m. of 0% glucose (black) or 6% D-glucose (grey). Error bars, s.e.m. Pairwise Student's *t* test was used to compare values to the Col-0. *, $P < 0.05$; **, $P < 0.01$. 35S:: represents a constitutive promoter from the cauliflower mosaic virus used here for ectopic overexpression of the indicated open reading frame. *n* (the number of independent experiments) = 2 for 0%, 4 for 6% or 3 for the other concentrations of D-glucose.

changes such as the positions and strengths of glucose sinks such as roots, meristems and fruits[35]. Yeasts, similarly to plants, adopt growth strategies based over wide swings in glucose levels and do so, in part, through a G-protein-coupled signalling pathway[36–38]. However, the level of glucose must be sustained for the cell to commit to an altered growth strategy.

Whereas the rate-limiting step for G-protein activation in humans is 7TM-receptor-catalysed nucleotide exchange, this process is spontaneous for the *Arabidopsis* Gα protein[3,7]. Plant cells must therefore use accessory control to keep the complex in the basal state until self-activation is permitted. The protein prototype 7TM-GAP, AtRGS1, serves as a receptor or co-receptor for glucose (and/or glucose metabolites) and accelerates the intrinsic hydrolysis of its cognate Gα subunit, AtGPA1 (refs 3,8) to keep the complex in its basal state[39].

WNKs may play a role in circadian and developmental timing in *Arabidopsis*[40–42] and in abiotic stress[43,44], but until now, no specific biochemical pathway was known, although recently, human WNK1 was shown to coordinate signalling through PIP2 and Gq-coupled pathways by an interesting dual mechanism[45]. Of particular interest here is that WNK1 promotes clathrin-dependent endocytosis of renal ion transporters and potassium channels[46], suggesting by comparison with AtWNK8 that the regulatory role of WNK in membrane protein trafficking is its primordial function.

In animals, internalization of 7TM GPCRs desensitizes cells to the receptor agonists (Fig. 7a–c); however, recent data indicate that, in some cases, signalling subsequent to endocytosis occurs at the endosome[2,47]. The results from our epistasis analyses here prompt us to propose that AtRGS1 mediates sugar signalling through both the endosome and the G protein at the plasma membrane. For example, for many sugar phenotypes, the loss-of-function alleles of the G-protein complex (*gpa1*, *agb1* or *agg1*/*agg2*) and *AtWNK8* exhibit the opposite phenotype to the *rgs1* mutants, suggesting that AtWNK8-mediated AtRGS1 endocytosis drives G-protein activation at the plasma membrane. In contrast, null alleles of *gpa1*, *agb1*, *rgs1* and *wnk8/10* all abrogate signalling as measured by *TBL26* (and several others) expression, implying that internalized AtRGS1 transmits signals from the endosome.

Here we show that glucose-induced endocytosis of AtRGS1 is achieved by AtWNK8-mediated phosphorylation of at least two C-terminal serines. Although we show the elements, order and mechanism of this process, the cause of the instantaneous G protein activation that leads to the sustained activation mechanism we elucidate

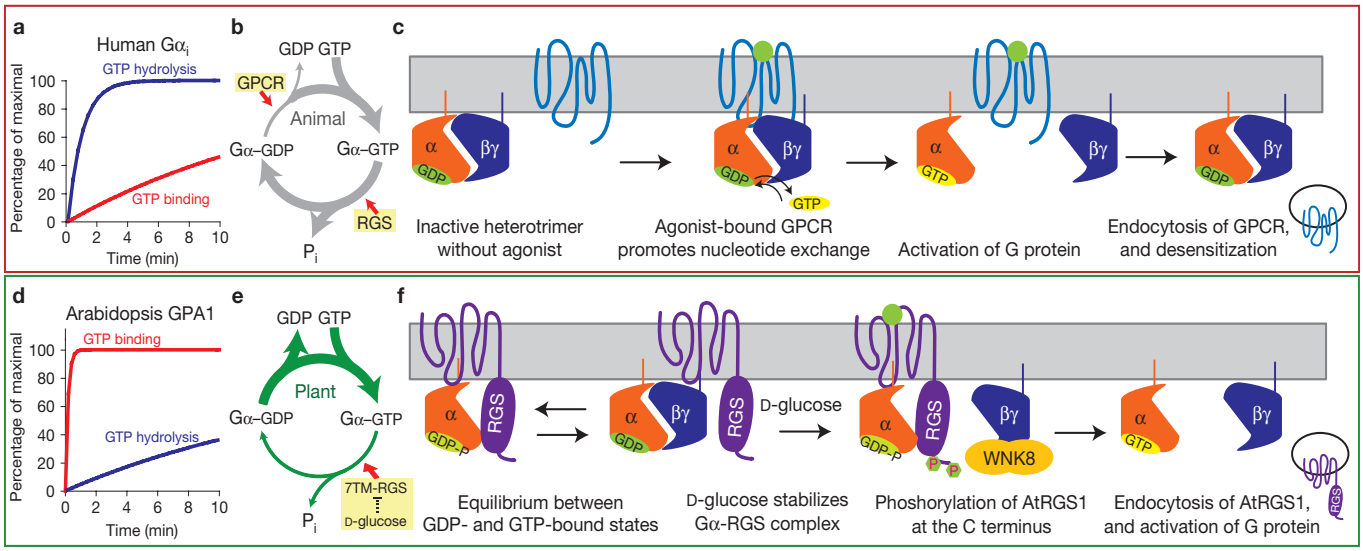

Figure 7 Model of sustained G-protein activation in *Arabidopsis*; comparison of activation mechanisms between fast and slow nucleotide exchanging G proteins. (**a**,**d**) The rate of guanine nucleotide exchange of human G protein is slower than that of GTP hydrolysis. However, *Arabidopsis* AtGPA1 rapidly releases GDP, whereas GTP hydrolysis is slow. (**b**,**e**) On the basis of these intrinsic properties, human G proteins require GPCRs to form the active GTP-bound state. In contrast, AtGPA1 requires a constitutively active 7TM-RGS protein, AtRGS1, to keep the inactive GDP-bound state. Genetic evidence suggests that D-glucose inhibits AtRGS1 to activate the *Arabidopsis* G-protein pathway. (**c**,**f**) Many human GPCRs are endocytosed after phosphorylation and subsequent endocytosis causes desensitization of G protein signalling. In *Arabidopsis*, in the absence of glucose, Gα subunit binding is in equilibrium between the RGS and Gβ dimerization interfaces, both shared on the Gα subunit. Glucose shifts the equilibrium towards the Gα–RGS dimer increasing the time the Gβγ remains free from the heterotrimer. The free Gβγ dimer recruits AtWNK8 to phosphorylate AtRGS1 at its C terminus. Phosphorylation is requisite for AtRGS1 endocytosis. Endocytosis causes uncoupling of AtGPA1 from its inhibitor, AtRGS1, and subsequent sustained activation of G-protein signalling.

here remains unclear. Figure 7 illustrates a model that summarizes the key findings and our interpretation: in the absence of glucose stimulation, the plant self-activating Gα protein (Fig. 7d,e) cycles between the GTP- and GDP-bound states with its binding partners, Gβγ and AtRGS1 (Fig. 7e,f). The GTPase-accelerating activity of AtRGS1 promotes inactive heterotrimer formation whereas the self-activating property of AtGPA1 promotes association with AtRGS1 (ref. 3). The newly freed Gβγ dimer recruits AtWNK8 to the plasma membrane to phosphorylate the C terminus of AtRGS1. Once phosphorylated, AtRGS1 undergoes endocytosis and the Gα protein is physically uncoupled from its negative regulator, left to self-activate at the plasma membrane. Each signalling component, both endosomal AtRGS1 and plasma-membrane-delimited Gα and Gβγ, consequently relays signals for a sustained response to the sugar signal. The initial mechanism of *Arabidopsis* G-protein activation is still unknown, but we previously reported that the D-glucose stimulation increased AtGPA1 association with AtRGS1 (ref. 3). As the RGS domain and Gβ have overlapping interaction interfaces on the Gα protein surface[48,49], increased association between AtGPA1 and AtRGS1 would preclude heterotrimer formation and favour Gβγ release (Fig. 7f). An alternative hypothesis is that glucose may directly inhibit the GAP activity of AtRGS1, thus permitting Gα self-activation and heterotrimer dissociation. Although glucose has no effect *in vitro* on the GAP activity of the RGSbox + Ct of AtRGS1 (Supplementary Fig. S7c,d), it remains possible that sugar directly regulates GAP activity in the full-length protein or indirectly by conformation changes promoting GAP activity. Both hypotheses are consistent with the glucose-induced change in FRET efficiency between AtGPA1 and AtRGS1 (ref. 3).

Sustained plant G-protein activation is regulated in an opposite manner as in animals (Fig. 7). Despite the contrasting mechanisms of G-protein activation between plant and animal cells, there is an intriguing similarity in the requirement for phosphorylation in GPCR endocytosis. Although we elucidated the critical role of C-terminal phosphorylation of AtRGS1 for its endocytosis and provide a mechanism for sustained G protein-dependent signalling, we raised questions of whether trafficking mechanisms of mammals and of *Arabidopsis* 7TM proteins (for example, GPCRs versus 7TM-RGS) share evolutionary history, and how *Arabidopsis* and mammals independently combined similar functional compatibilities from different gene products to evolve receptor-trafficking mechanisms. □

METHODS

Methods and any associated references are available in the online version of the paper.

Note: Supplementary Information is available in the online version of the paper

ACKNOWLEDGEMENTS

We thank D. Smalley for determining the phosphorylation sites of AtRGS1, N. Nakamichi, T. Eulgem and H. Ma (Pennsylvania State University, USA) for supplying experimental materials, K. Williamson and M. Mathew for assistance in protein purification and gene cloning, A. Urano for assisting in experiments and H. Dohlman for helpful discussions. This work was supported by grants from the NIGMS (R01GM065989) and NSF (MCB-0723515 and MCB-0718202) to A.M.J. The Division of Chemical Sciences, Geosciences, and Biosciences, Office of Basic Energy Sciences of the US Department of Energy through grant DE-FG02-05er15671 to A.M.J. financially supported the genotyping of the materials in this study.

AUTHOR CONTRIBUTIONS

A.M.J. and J.H. made the initial observation of glucose-dependent AtRGS1 internalization. J.H., J.G. and J.P.T. characterized the sugar dependence of

endocytosis of wild-type and mutant AtRGS1 (Fig. 1). N.P. quantified endocytosis of AtRGS1 in mutant genotypes and performed FRET analyses and co-localization of AtRGS1 with compartment markers. J.C.J. assisted in the initial intrinsic tryptophan fluorescence measurement. J.Y. assisted in the real-time PCR experiments. D.U. designed most of the experiments, performed all of the biochemical and physiological analyses, performed some of the BiFC experiments and analyses, performed all the gene expression profiling and constructed all the expression vectors. A.M.J., D.U. and N.P. wrote the manuscript. All authors edited the manuscript.

COMPETING FINANCIAL INTERESTS

The authors declare no competing financial interests.

Published online at www.nature.com/doifinder/10.1038/ncb2568
Reprints and permissions information is available online at www.nature.com/reprints

1. Kohout, T. A. & Lefkowitz, R. J. Regulation of G protein-coupled receptor kinases and arrestins during receptor desensitization. *Mol. Pharmacol.* **63,** 9–18 (2003).
2. Hanyaloglu, A. C. & von Zastrow, M. Regulation of GPCRs by endocytic membrane trafficking and its potential implications. *Annu. Rev. Pharmacol. Toxicol.* **48,** 537–568 (2008).
3. Johnston, C. A. *et al.* GTPase acceleration as the rate-limiting step in *Arabidopsis* G protein-coupled sugar signaling. *Proc. Natl Acad. Sci. USA* **104,** 17317–17322 (2007).
4. Urano, D. *et al.* G protein activation without a GEF in the plant kingdom. *PLoS Genet.* **8,** e1002756 (2012).
5. Gookin, T. E., Kim, J. & Assmann, S. M. Whole proteome identification of plant candidate G-protein coupled receptors in *Arabidopsis*, rice, and poplar: Computational prediction and *in-vivo* protein coupling. *Genome Biol.* **9,** R120 (2008).
6. Moriyama, E. N., Strope, P. K., Opiyo, S. O., Chen, Z. & Jones, A. M. Mining the *Arabidopsis thaliana* genome for highly-divergent seven transmembrane receptors. *Genome Biol.* **7,** R96 (2006).
7. Jones, J. C. *et al.* The crystal structure of a self-activating G protein alpha subunit reveals its distinct mechanism of signal initiation. *Sci. Signal* **4,** ra8 (2011).
8. Chen, J. G. *et al.* A seven-transmembrane RGS protein that modulates plant cell proliferation. *Science* **301,** 1728–1731 (2003).
9. Ullah, H. *et al.* The β-subunit of the *Arabidopsis* G protein negatively regulates auxin-induced cell division and affects multiple developmental processes. *Plant Cell* **15,** 393–409 (2003).
10. Ullah, H. *et al.* Modulation of cell proliferation by heterotrimeric G protein in *Arabidopsis*. *Science* **292,** 2066–2069 (2001).
11. Trusov, Y. *et al.* Heterotrimeric G protein gamma subunits provide functional selectivity in Gβγ dimer signaling in *Arabidopsis*. *Plant Cell* **19,** 1235–1250 (2007).
12. Chakravorty, D. *et al.* An atypical heterotrimeric G protein gamma subunit is involved in guard cell K(+) channel regulation and morphological development in *Arabidopsis thaliana*. *Plant J.* **67,** 840–851 (2011).
13. Chen, J. G., Gao, Y. & Jones, A. M. Differential roles of *Arabidopsis* heterotrimeric G-protein subunits in modulating cell division in roots. *Plant Physiol.* **141,** 887–897 (2006).
14. Chen, J. G. & Jones, A. M. AtRGS1 function in *Arabidopsis thaliana*. *Methods Enzymol.* **389,** 338–350 (2004).
15. Booker, K. S., Schwarz, J., Garrett, M. B. & Jones, A. M. Glucose attenuation of auxin-mediated bimodality in lateral root formation is partly coupled by the heterotrimeric G protein complex. *PLoS One* **5,** e12833 (2010).
16. Grigston, J. C. *et al.* D-Glucose sensing by a plasma membrane regulator of G signaling protein, AtRGS1. *FEBS Lett.* **582,** 3577–3584 (2008).
17. Pego, J. V. & Smeekens, S. C. Plant fructokinases: A sweet family get-together. *Trends Plant Sci.* **5,** 531–536 (2000).
18. Sherson, S. M., Alford, H. L., Forbes, S. M., Wallace, G. & Smith, S. M. Roles of cell-wall invertases and monosaccharide transporters in the growth and development of *Arabidopsis*. *J. Exp. Bot.* **54,** 525–531 (2003).
19. Valpuesta, V. & Botella, M. A. Biosynthesis of L-ascorbic acid in plants: new pathways for an old antioxidant. *Trends Plant Sci.* **9,** 573–577 (2004).
20. Chen, Z. *et al.* Expression analysis of the AtMLO gene family encoding plant-specific seven-transmembrane domain proteins. *Plant Mol. Biol.* **60,** 583–597 (2006).
21. Chen, Z. *et al.* Two seven-transmembrane domain Mildew Resistance Locus O proteins cofunction in *Arabidopsis* root thigmomorphogenesis. *Plant Cell* **21,** 1972–1991 (2009).
22. Hislop, J. N. & von Zastrow, M. Role of ubiquitination in endocytic trafficking of G-protein-coupled receptors. *Traffic* **12,** 137–148 (2011).
23. Hislop, J. N. & Zastrow, M. in *Regulated Membrane Trafficking and Proteolysis of GPCRs The G Protein-Coupled Receptors Handbook* (ed. Devi, L. A.) 95–105 (Humana Press, 2005).
24. Marchese, A., Paing, M. M., Temple, B. R. & Trejo, J. G protein-coupled receptor sorting to endosomes and lysosomes. *Annu. Rev. Pharmacol. Toxicol.* **48,** 601–629 (2008).
25. Klopffleisch, K. *et al. Arabidopsis* G-protein interactome reveals connections to cell wall carbohydrates and morphogenesis. *Mol. Syst. Biol.* **7,** 532 (2011).
26. Nelson, B. K., Cai, X. & Nebenfuhr, A. A multicolored set of in vivo organelle markers for co-localization studies in *Arabidopsis* and other plants. *Plant J.* **51,** 1126–1136 (2007).
27. Moore, M. J., Soltis, P. S., Bell, C. D., Burleigh, J. G. & Soltis, D. E. Phylogenetic analysis of 83 plastid genes further resolves the early diversification of eudicots. *Proc. Natl Acad. Sci. USA* **107,** 4623–4628 (2010).
28. Stubbs, M. D. *et al.* Purification and properties of *Arabidopsis thaliana* type 1 protein phosphatase (PP1). *Biochim. Biophys. Acta* **1550,** 52–63 (2001).
29. Seki, M. *et al.* Functional annotation of a full-length *Arabidopsis* cDNA collection. *Science* **296,** 141–145 (2002).
30. Day, P. W., Wedegaertner, P. B. & Benovic, J. L. Analysis of G-protein-coupled receptor kinase RGS homology domains. *Methods Enzymol.* **390,** 295–310 (2004).
31. Lalonde, S. *et al.* A membrane protein/signaling protein interaction network for *Arabidopsis* version AMPv2. *Front Physiol.* **1,** 24 (2010).
32. Huang, C. L., Cha, S. K., Wang, H. R., Xie, J. & Cobb, M. H. WNKs: protein kinases with a unique kinase domain. *Exp. Mol. Med.* **39,** 565–573 (2007).
33. Chen, J. G. *et al.* RACK1 mediates multiple hormone responsiveness and developmental processes in *Arabidopsis*. *J. Exp. Bot.* **57,** 2697–2708 (2006).
34. Deuschle, K. *et al.* Rapid metabolism of glucose detected with FRET glucose nanosensors in epidermal cells and intact roots of *Arabidopsis* RNA-silencing mutants. *Plant Cell* **18,** 2314–2325 (2006).
35. Lalonde, S., Wipf, D. & Frommer, W. B. Transport mechanisms for organic forms of carbon and nitrogen between source and sink. *Annu. Rev. Plant Biol.* **55,** 341–372 (2004).
36. Lemaire, K., Van de Velde, S., Van Dijck, P. & Thevelein, J. M. Glucose and sucrose act as agonist and mannose as antagonist ligands of the G protein-coupled receptor Gpr1 in the yeast *Saccharomyces cerevisiae*. *Mol. Cell* **16,** 293–299 (2004).
37. Isshiki, T., Mochizuki, N., Maeda, T. & Yamamoto, M. Characterization of a fission yeast gene, gpa2, that encodes a G alpha subunit involved in the monitoring of nutrition. *Genes Dev.* **6,** 2455–2462 (1992).
38. Versele, M., de Winde, J. H. & Thevelein, J. M. A novel regulator of G protein signalling in yeast, Rgs2, downregulates glucose-activation of the cAMP pathway through direct inhibition of Gpa2. *Embo J.* **18,** 5577–5591 (1999).
39. Jones, J. C., Temple, B. R., Jones, A. M. & Dohlman, H. G. Functional reconstitution of an atypical G protein heterotrimer and regulator of G protein signaling protein (RGS1) from *Arabidopsis thaliana*. *J. Biol. Chem.* **286,** 13143–13150 (2011).
40. Murakami-Kojima, M., Nakamichi, N., Yamashino, T. & Mizuno, T. The APRR3 component of the clock-associated APRR1/TOC1 quintet is phosphorylated by a novel protein kinase belonging to the WNK family, the gene for which is also transcribed rhythmically in *Arabidopsis thaliana*. *Plant Cell Physiol.* **43,** 675–683 (2002).
41. Park, H. Y. *et al.* EMF1 interacts with EIP1, EIP6 or EIP9 involved in the regulation of flowering time in *Arabidopsis*. *Plant Cell Physiol.* **52,** 1376–1388 (2011).
42. Wang, Y. *et al.* The plant WNK gene family and regulation of flowering time in *Arabidopsis*. *Plant Biol (Stuttg)* **10,** 548–562 (2008).
43. Wang, Y., Suo, H., Zhuang, C., Ma, H. & Yan, X. Overexpression of the soybean GmWNK1 altered the sensitivity to salt and osmotic stress in *Arabidopsis*. *J. Plant Physiol.* (2011).
44. Kumar, K., Rao, K. P., Biswas, D. K. & Sinha, A. K. Rice WNK1 is regulated by abiotic stress and involved in internal circadian rhythm. *Plant Signal Behav.* **6,** 316–320 (2011).
45. An, S. W. *et al.* WNK1 Promotes PIP2 synthesis to coordinate growth factor and GPCR-G(q) signaling. *Curr. Biol.* **21,** 1979–1987 (2011).
46. Huang, C. L., Yang, S. S. & Lin, S. H. Mechanism of regulation of renal ion transport by WNK kinases. *Curr. Opin. Nephrol. Hypertens.* **17,** 519–525 (2008).
47. Reiter, E., Ahn, S., Shukla, A. K. & Lefkowitz, R. J. Molecular mechanism of β-arrestin-biased agonism at seven-transmembrane receptors. *Annu. Rev. Pharmacol. Toxicol.* **52,** 179–197 (2011).
48. Tesmer, J. J., Berman, D. M., Gilman, A. G. & Sprang, S. R. Structure of RGS4 bound to AlF4–activated G(i α1): stabilization of the transition state for GTP hydrolysis. *Cell* **89,** 251–261 (1997).
49. Lambright, D. G. *et al.* The 2.0 A crystal structure of a heterotrimeric G protein. *Nature* **379,** 311–319 (1996).

METHODS

Plant materials. The *gpa1-3*, *agb1-2*, *gpa1-4 agb1-2* double, *gpa1-4 agb1-2 agg1-1 agg2-1* quadruple, *rgs1-1* and *rgs1-2* mutants were described previously[8–11]. The 35S:: AtGPA1^{Q222L} *gpa1*-4, 35S::AtGPA1 *gpa1*-4 and 35S::AGB1 agb1-2 lines were previously generated[9,10]. The 35S::AtWNK8 line was provided by T. Eulgem (UC Riverside, USA). *wnk1*, *wnk8-1*, *wnk8-2*, *wnk10-1* and *wnk10-2* mutants were obtained from the Arabidopsis Biological Resource Center (ABRC) stock centre (SALK_015778, SALK_103318, SALK_024887, SALK_012899 and SALK_071328C). All DNA-insertion lines were made homozygous and the transfer DNA insertions were confirmed by PCR of genomic DNA with the following primer sets; wnk8 − 1_RP: 5′-TGCCATGAATTCAGGAGTACC-3′, *wnk8* − 1_LP: 5′-AAAGATCCTTCTGGCCGTTAC-3′, *wnk8* − 2_RP: 5′-TACTCCTGAATTCATGGCACC-3′, *wnk8* − 2_LP: 5′-CAGCAGATCTTGGAAGG-ACTG-3′, *wnk1*_RP: 5′-CGCAAGACATTCTTCGAATTC-3′, *wnk1*_LP: 5′-GGGAATCAAGGAGAGGTCAAG-3′, *wnk10*_RP: 5′-TGCTCTTCTGCTAAAAG-CAGC-3′, *wnk10*_LP: 5′-GGGTCCATTCCTCTCTCTCAG-3′ and transfer DNA_LB: 5′-ATTTTGCCGATTTCGGAAC-3′ (Supplementary Fig. S3e).

Transient expression in plants. Transient expression in tobacco was as described previously[50] with the following modifications to the infiltration buffer (10 mM $MgCl_2$, 10 mM MES and 200 μM acetosyringone). *Agrobacterium tumefacien* was incubated in infiltration solution for at least 4 h. Images were typically captured 3 days after inoculation to obtain the lowest detectable level of expression. Transient expressions in *Arabidopsis* seedlings were as described previously[51]. Equal volumes of the *A. tumefacien* ($D_{600\,nm} = 1.0$) harbouring the plasmids were mixed just before the dipping step in the *Arabidopsis* transformation protocol.

BiFC was performed using 4–5 week-old tobacco leaves that were infected with *A. tumefacien* to express nYFP- and cYFP-tagged proteins as described previously[16] except with the following modifications. pENTR clones of the genes of interest were subcloned into one or more of the BiFC vectors pBatTL–sYFP-N or pBatTL–sYFP-C (for C-terminal tagged nYFP and cYFP halves, respectively) and pCL112_JO or pCL113_JO (for N-terminal tagged nYFP and cYFP halves, respectively). An internal positive transformation control (mitochondrial RFP marker; Mt-rk obtained from the ABRC (CD3-991)) was included to address the issue of transgene silencing (p19 gene silencing suppressor, mt-rk and two BiFC halves).

Plasmids, recombinant proteins and antibodies. Complementary DNA for *AtWNK1* was obtained from N. Nakamichi (Nagoya University, Japan), and cDNAs for *AtWNK8* and *AtWNK10* were obtained from the ABRC. *AtWNK* coding sequences were subcloned into pDEST15 (N-terminal GST), pCL113_JO (N-terminal split-cYFP), pACTGW–attR and pB7WGC2 (N-terminal CFP). *Ara7*, *Rha1*, *RabA5d*, *VTI11* and *SYP23* were obtained from the ABRC and subcloned into pEarleyGate101 (C-terminal YFP–HA), pEarleyGate102 (C-terminal CFP), and pEarleyGate104 (N-terminal YFP) plasmids. *AtRGS1* (encoding amino acids 1–459) and its C-terminal truncated mutant (encoding amino acids 1–416, designated as AtRGS1-ΔCt) were subcloned to pEarleyGate205 (C-terminal TAP), pEarleyGate101 and pBAT–TL–B–sYFP-N (C-terminal split-nYFP). Coding sequences for the cytoplasmic region of AtRGS1 were synthesized by Celtek Bioscience (Nashville) with codons optimized for expression in *Escherichia coli*. AtRGS1-coding sequences RGS box + Ct (amino acids 284–459), RGS box (amino acids 284–416) and Ct (amino acids 400–459) of AtRGS1 were subcloned into pENTR–TEV–TOPO, pAS–attR and pDEST17 (N-terminal His) or pDEST15. AtRGS1$^{\Delta CtSA}$ (amino acids 1–416, S405A/S406A) was generated with QuikChange by direct mutagenesis. Recombinant GST- or His-tagged proteins were expressed in *E. coli* (ArcticExpress RP, Agilent Technologies) with 0.5 mM IPTG at 12 °C, solubilized in buffer A (50 mM Tris–HCl (pH 7.5), 100 mM NaCl, 5 mM 2-mercaptoethanol, 1 mM phenylmethylsulphonyl fluoride (PMSF) and 1 μg ml^{-1} leupeptin) with 0.25 mg ml^{-1} lysozyme and 0.2% NP-40, purified from the soluble fraction using glutathione–Sepharose 4B (GE Healthcare) or TALON metal-affinity resin (Clonetech), washed with buffer A containing 500 mM NaCl and 0.1% sodium cholate, and eluted with 20 mM glutathione or 500 mM imidazole, respectively. For His-tagged proteins, 5 mM imidazole was included in crude extracts to reduce nonspecific binding. The purified proteins were dialysed in buffer B (20 mM Tris–HCl (pH 7.5), 50 mM NaCl, 1 mM $MgCl_2$, 1 mM EDTA, 1 mM dithiothreitol (DTT) and 1 mM PMSF).

The AtGPA1 and AGB1 antibodies were described previously[10,52]. The AtRGS1 and phosphor-specific AtRGS1 antisera were raised with the His-tagged RGS1 box + Ct protein or the phosphorylated AtRGS1 peptide (amino acids 424–440): CKEGY–pS–FSSPRL–pS–pS–VQGS (pS; phosphorylated-serine; Yen-Zym Antibodies). The anti-phospho-AtRGS1 antibody was purified by affinity chromatography using the phosphorylated AtRGS1 peptide conjugated to an affinity matrix. The purified antibody was further cleaned up with unphosphorylated-AtRGS1 peptide (amino acids 424–440) to remove phosphorylation-independent AtRGS1 antibody. The specificity of the antibody against phosphorylated- and unphosphorylated-AtRGS1 peptides was checked with an enzyme-linked immunosorbent assay.

Microscopies. Vertical optical sections (*Z* stacks) of hypocotyl epidermal cells of dark-grown seedlings located approximately 3–4 mm from the cotyledon were imaged using a Zeiss LSM710 confocal laser scanning microscope equipped with a Plan-NeoFluor ×20/0.5 objective and a C-Apochromat ×40/1.20 water immersion objective. YFP, CFP and RFP were excited by a 514 nm and 458 nm argon laser and a 560 nm diode laser, respectively, and their respective emissions were detected at 526–569, 460–520 and 565–621 nm by a photomultiplier detector. The digital images were analysed with Zen software (Zeiss).

Some fluorescence images of tobacco transients and *Arabidopsis* seedlings were captured using an Olympus IX81 inverted microscope (Olympus America) with a Hamamatsu CCD (charge-coupled device) C4742-80-12AG (Hamamatsu Photonics) and analysed using Slidebook 5.0 (3i). Filter sets used were: YFP (excitation, 500/20 nm; emission, 535/30 nm; same filter for GFP-tag), CFP (excitation, 436/20 nm; emission, 480/40 nm).

FRET measurements in CFP/YFP double-labelled cells were determined by the acceptor photobleaching method. The intracellular region of interest varied in size depending on the substructure analysed but fell into two categories: initial regions at or adjacent to the plasma membrane, and regions inside the cell or not adjacent to the plasma membrane. The laser intensity and duration were optimized to achieve at least 80% YFP photobleaching without affecting donor emission quantum yield. CFP and YFP were excited by the 458 nm and 514 nm lines of an argon laser, respectively. Emissions were detected at 460–520 and 526–569 nm. Pre- ($I_{pre.\lambda}$) and post-bleaching ($I_{post.\lambda}$) fluorescence intensities of both CFP and YFP were obtained and the FRET efficiencies in the region of interest were calculated using the following equation:

$$\text{FRET Eff} = \frac{I_{post.\lambda} - I_{pre.\lambda}}{I_{post.\lambda}}$$

The digital images and FRET analysis were analysed with Zen software (Zeiss).

Quantification and statistics. Fluorescence quantification was obtained using the software ImageJ[53]. Randomly selected hypocotyl images from at least five whole *Z*-section image stacks from three independent experiments were selected for quantification. Images were thresholded for fluorescence signal before selecting regions. Outlined regions of fluorescence signal from within cells were selected and subtracted from the total hypocotyl fluorescence of the hypocotyl in the image (fluorescence not in the hypocotyl was excluded from measurements). Outlined regions were chosen distant from the cell periphery as determined in the bright-field/differential interference contrast images.

Statistical comparison of mean fluorescence was performed using analysis of variance to confirm differences in treatments and genotypes followed by mean analysis by Tukey's test. Typically, a minimum of five *Z* sections of the root were randomly selected and used for quantification. There is little variation between different *Z* sections of cells in the scan range, which was typically 20–30 nm from root surface.

***In vitro* co-precipitations.** Seventy-five pmol of His–RGS box + Ct and 50 pmol of GST–AtWNK kinases were mixed with 10 μl of glutathione–Sepharose 4B (GE Healthcare) in 250 μl of buffer C (50 mM MES (pH 6.0), 10 mM $MgCl_2$, 5 mM $MnCl_2$, 2 mM DTT, 1 mM PMSF and 1 μg ml^{-1} leupeptin). The tubes were rotated for 60 min at 4 °C, and the resin was washed with buffer C with 0.1% NP-40 four times. The co-precipitated or input proteins were visualized by immunoblot analysis with anti-AtRGS1 antisera and Coomassie brilliant blue (CBB) staining. To test binding with AtGPA1, the same procedure was followed except that 50 μM GDP with or without aluminium tetrafloride (30 μM $AlCl_3$, 10 mM $MgCl_2$ and 5 mM NaF) was added into buffer C.

Yeast two-hybrid assays. pAS–RGS box + Ct, RGS box or Ct of AtRGS1 and pACTGW–AtWNK1, AtWNK8 or AtWNK10 were transformed into AH109 yeast cells. The colonies grown on SD (-LW) plates were inoculated into SD (-LW) liquid media and cultured overnight at 30 °C. The β-galactosidase activity of the yeast was determined according to the manufacturer's instruction (Clonetech).

Physiological assay. Approximately 40 seeds of *Arabidopsis* were sterilized, vernalized and sown on 1/2 × MS plates containing 0%, 4%, 5% and 6% D-glucose. The plates were incubated at 23 °C under continuous light (50 μmol s^{-1} m^{-2}) for 10 days. The number of green seedlings was divided by the number of germinated seeds. The score was presented with s.e.m.

DOI: 10.1038/ncb2568

***In vitro* and *in vivo* phosphorylation assays.** Seventy-five pmol of His–RGS box + Ct, –RGS box or GST–AtRGS1-Ct was incubated with 0.05 pmol of GST, GST–AtWNK1, GST–AtWNK8 or 5.0 pmol GST–AtWNK10 in 15 µl of buffer C containing 0.2 mM [γ-^{32}P]ATP for 6 h at room temperature. The reactions were terminated by adding Laemmli sample buffer and the proteins were separated by SDS–PAGE. Incorporation of ^{32}P into the separated proteins was visualized with a phosphor screen (Molecular Dynamics).

Approximately 50 sterilized and stratified seeds were grown in 1/2 × MS liquid media with 1% sucrose at 23 °C, at 100 r.p.m. under low light (50 µmol s^{-1} m^{-2}) conditions. After 7 days in culture, the seedlings were starved of sugars with 1/2 × MS media lacking sucrose for 2 days in a dark chamber, and then stimulated with 6% D-glucose, 100 nM calyculin A and 10 mM sodium orthovanadate, as indicated. The seedlings were frozen, powdered with a mortar and pestle and then lysed with buffer D (150 mM Tris–HCl (pH 7.5), 300 mM NaCl, 20% glycerol, 5 mM DTT, 2 mM Na_3VO_4, 10 mM NaF, 20 mM β-glycerophosphate, 1 mM PMSF, 2 µg ml^{-1} leupeptin and 1% ASB-14). After 2 h incubation at 4 °C, the lysates were centrifuged and the supernatants were subjected to SDS–PAGE and immunoblot analysis. The phosphorylated AtRGS1 was detected with anti-phospho-RGS1 antibody. The total amount of AtRGS1–TAP was determined with peroxidase anti-peroxidase soluble complex (PAP). To observe a band shift of AtRGS1–TAP, AtRGS1$^{\Delta CtSA}$–TAP or AtGPA1, total extracts were separated on a 12.5% Anderson's gel[54] and subjected to SDS–PAGE and immunoblot analyses using PAP or anti-AtGPA1 antisera.

Quantitative real-time PCR. Approximately 150 seeds were grown in 1/2 × MS liquid media with 1% glucose at 23 °C with low light (50 µmol s^{-1} m^{-2}) conditions. After 7 days in culture, the seedlings were starved with 1/2 × MS media for 2 days in the dark. Then, seedlings were stimulated with 6% sugar for 3 h in dark conditions. The messenger RNA and cDNA were prepared with RNAeasy (Qiagen) and Superscript III (Invitrogen) according to the manufacturer's instructions. Expression of *TBL26* and *TUB4* was analysed by real-time PCR with SYBRgreen or Taqman probes using the following primer and probe sets: TBL26 forward, 5′-CGCCATCGAACCTTCGTCAAATTC-3′; TBL26 reverse, 5′-TCGTCCATTCAATAGGCAGTTCTGA-3′; TBL26 Taqman, 5′-CTCCCGGAAACGTTTCATCAGCAAAG-3′; TUB4 forward, 5′-AGAGGTTGACGAGCAGATGA-3′; TUB4 reverse, 5′-ACCAATGAAAGTAGACGCCA-3′; TUB4 Taqman, 5′-CCCAAACAACGTCAAGTCCAGTGTCTGT-3′.

Mass spectrometry. Phosphorylated protein bands were excised from 10% polyacrylamide gels (Biorad) and digested as described previously[55]. The trypsinized peptides were analysed by matrix-assisted laser desorption/ionization tandem time-of-flight mass spectrometry and by liquid chromatography-electrospray ionization–tandem mass spectrometry. A 90-min gradient was used and MS analysis was performed with an LTQ Orbitrap XL mass spectrometer (ThermoFisher Scientific). Peptide masses were queried using the MASCOT algorithm against the non-redundant NCBI database and the AtRGS1-specific database with possible phosphorylation sites. On the basis of the MASCOT results, two phosphorylated peptides (EGYSFSSPR and LSSVQGSDDPFYQEHMSK) were identified. On the basis of manual inspection of the spectra, the phosphorylation sites were defined.

Accession numbers. RGS1, AT3G26090; TBL26, AT4G01080; WNK8, AT5G41990; WNK1, AT3G04910; WNK10, AT1G64630; GPA1, AT2G26300; AGB1, AT4G34460; AGG1, AT3G63420; AGG2, AT3G22942; Ara7, AT4G19640; Rha1, AT5G45130; RabA5d, AT2G31680; VTI11, AT5G39510; SYP23, AT4G17730; TUB4, AT5G44340; MLO6, AT1G61560. Mutant alleles for the genes were generated from the indicated T-DNA insertion lines: *wnk1* SALK_015778 *wnk8-1* SALK_103318 *wnk8-2* SALK_024887 *wnk10-1* SALK_012899 *wnk10-2* SALK_071328.

50. Sparkes, I. A., Runions, J., Kearns, A. & Hawes, C. Rapid, transient expression of fluorescent fusion proteins in tobacco plants and generation of stably transformed plants. *Nat. Protoc.* **1,** 2019–2025 (2006).
51. Grefen, C. *et al.* A ubiquitin-10 promoter-based vector set for fluorescent protein tagging facilitates temporal stability and native protein distribution in transient and stable expression studies. *Plant J.* **64,** 355–365 (2010).
52. Friedman, E. J. *et al.* Acireductone dioxygenase 1 (ARD1) is an effector of the heterotrimeric G Protein {β} subunit in *Arabidopsis*. *J. Biol. Chem.* **286,** 30107–30118 (2011).
53. Abramoff, M. D., Magalhaes, P. J. & Ram, S. J. Image processing with ImageJ. *Biophoton. Internat.* **11,** 36–42 (2004).
54. Anderson, C. W., Baum, P. R. & Gesteland, R. F. Processing of adenovirus 2-induced proteins. *J. Virol.* **12,** 241–252 (1973).
55. Hanna, S. L., Sherman, N. E., Kinter, M. T. & Goldberg, J. B. Comparison of proteins expressed by *Pseudomonas aeruginosa* strains representing initial and chronic isolates from a cystic fibrosis patient: an analysis by 2-D gel electrophoresis and capillary column liquid chromatography-tandem mass spectrometry. *Microbiology* **146** (Pt 10), 2495–2508 (2000).

DOI: 10.1038/ncb2568

nature cell biology

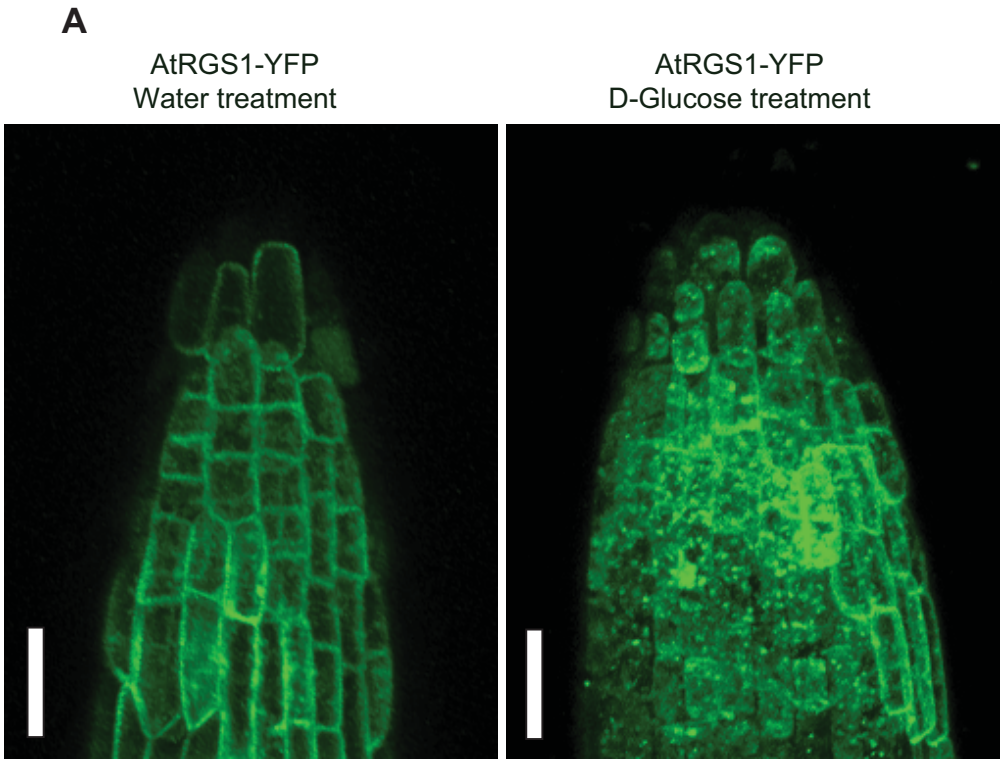

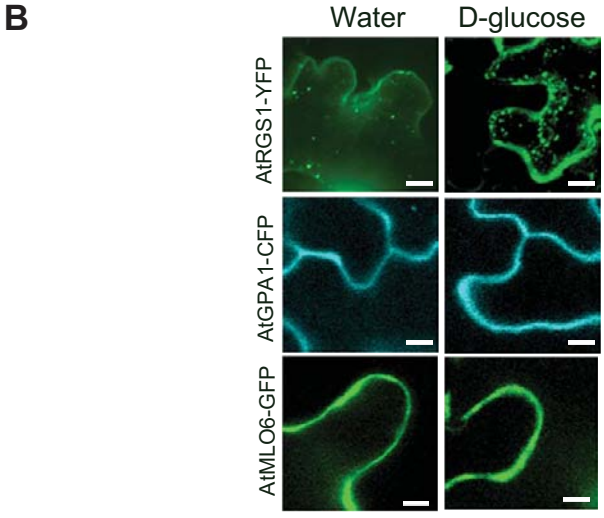

Figure S1 RGS1 internalization. (**A**) AtRGS1-YFP internalization at the root tip region after treatment with or without 6% D-glucose for 30 min. Scale bars = 20 μm (**B**) Sugar treatment of AtGPA1 and AtMLO6 in tobacco leaves. AtRGS1-YFP, AtGPA1-CFP or AtMLO6-GFP was expressed transiently in tobacco leaf epidermal cells. Disks of leaf tissue were treated with water or 6% D-glucose for 30 min prior to imaging; rotation at 40 rpm, 23ºC. Scale bars = 20 μm.

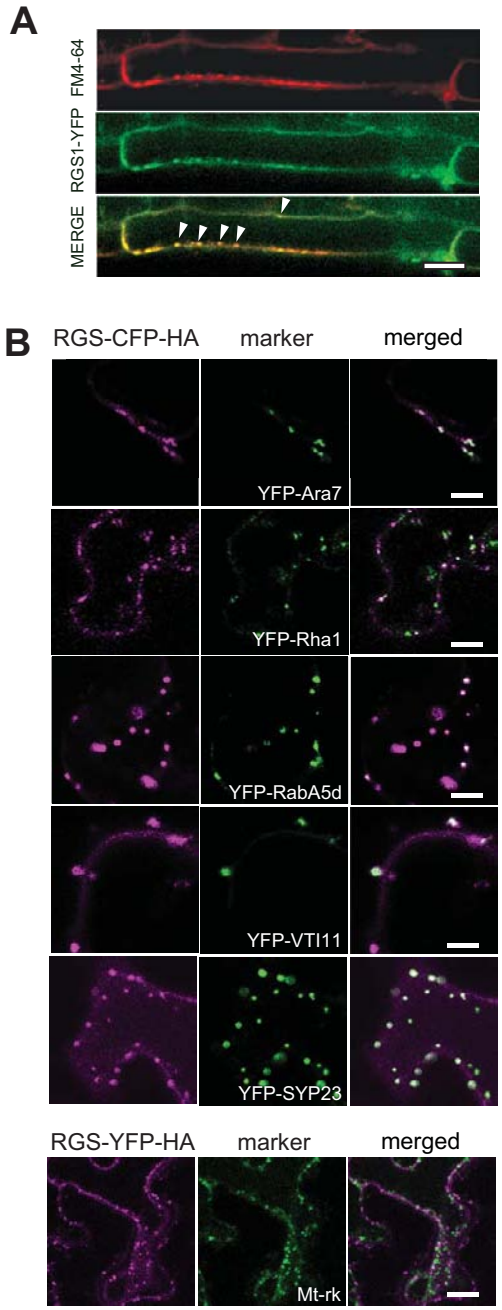

Figure S2 AtRGS1 internalizes into endosomal compartments. (**A**) AtRGS1 internalization coincides with the endocytic movement of FM4-64. Four-day-old AtRGS1-YFP expressing seedlings were treated with 6% D-glucose and chased with the FM4-64 endocytic marker for 30 min prior to imaging. AtRGS1 (green) can be seen co-localized with FM4-64 (red) in several compartments (arrow; white). Scale bars = 10 μm. (**B**) AtRGS1-CFP was transiently expressed in tobacco epidermal cells with various endosomal markers followed by treatment with 6% D-glucose for 30 min prior to imaging. Green fluorescing, late endosomal compartment markers are indicated (in middle column of panel triplets). AtRGS1-CFP is shown in the corresponding images (left column of panels). Co-localization (in white) at varying levels was seen in endosomal compartments marked by Ara7, Rha1, RabA5d, VTI11 and SYP23. Mt-RFP is a mitochondrial marker used as a non-endosomal control. Fluorescence was observed by confocal fluorescence microscopy as described in the *Methods*. Scale bars = 20 μm.

A	Y2H	Split - ubiquitin	BiFC	In vitro phospho rylation
AtPK1	YES		YES	NO
AtPK19	YES		YES	NO
LRRK	YES		YES	NO
WNK8	YES	YES	YES	YES

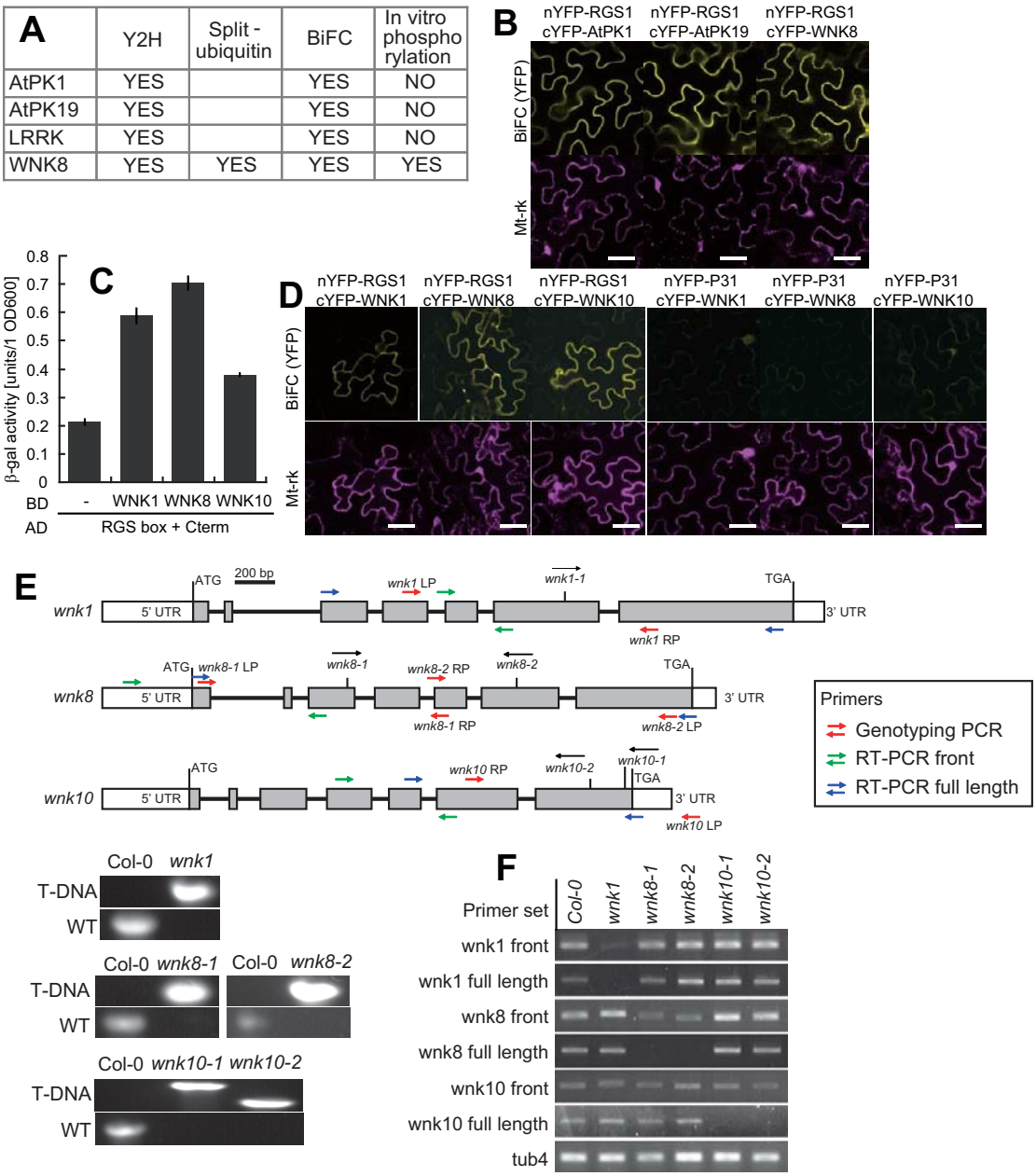

Figure S3 Identification of the AtRGS1 kinase. (**A**) Summary of the interaction screens using yeast two hybrid (split-ubiquitin) and Bimolecular Fluorescence Complementation (BiFC) and the *in vitro* kinase assay (In vitro phosphorylation). These assays were performed as described in the *Methods*. (**B**) *In vivo* interaction between AtRGS1 and kinases with BiFC. nYFP-tagged AtRGS1 was co-transformed with cYFP-tagged AtPK1, AtPK19, or AtWNK8 into tobacco leaves. Mt-rk is a RFP mitochondria marker (transformation control). Images of the complimented YFP (top panel, BiFC) and RFP control (lower panel, Mt-rk) fluorescence are shown. Fluorescence complementation of split YFP and expression of Mt-rk were observed by confocal fluorescence microscopy as described in the *Methods*. Scale bars = 50 μm. (**C**) Yeast two-hybrid assay between AtRGS1 and AtWNK kinases. Transformed yeast was grown in SD(-LW) liquid media and β-galactosidase activity in yeast was measured. Data shows mean and SEM from three independent experiments. (**D**) *In vivo* interaction between AtRGS1 and the AtWNKs. AtRGS1-nYFP or nYFP-P31 (control) was co-expressed with the indicated cYFP-AtWNK and the Mt-rk transformation control in tobacco leaves. Fluorescence complementation of split YFP and expression of Mt-rk are shown. Scale bars = 50 μm. (**E**) T-DNA insertion mutants of *AtWNK1*, *AtWNK8* and *AtWNK10*. Black arrows show the T-DNA insertion site and the arrow heads show the left border. Gray boxes represent exons. Red arrows indicate the position of primers used for genotyping. Genotyping is shown for the T-DNA insertion alleles or wild type gene as described in the *Methods*. (**F**) Genotyping and gene expression level. (**Left**) results for genotyping using the primers shown in E. with a primer from the left border of the T-DNA to determine insertion of the T-DNA (T-DNA) or without the T-DNA border to amplify the wild type allele (WT). All mutants are shown here to be homozygous at the indicated locus. Primes used for PCR are shown in the *Methods*. (**Right**) Transcription level of *AtWNK1*, *AtWNK8* and *AtWNK10* in their T-DNA insertion lines. Total RNA was prepared from seedlings of wild type Columbia or the T-DNA insertion lines, and DNA was synthesized with a reverse transcriptase and oligo dT primers. PCR products using primer sets shown in E were visualized on agarose gel. Primer sets used are AtWNK1 full length; GAAGGCATAGAAGTAGCATGG/ CTTCTTCTCTTCCTAACCCG, AtWNK1front; GCGTCGGGACTCCTGAGTTCAT/CGAGCAGAGACTCTAAGCGATACGG, AtWNK8 full length; GCCGAGAAAGATCCTTCTGG/ GCGTTCTCTATTGCATCCTC, AtWNK8 front; GGGGACCAAAATCAAAATCATGGTG/ TCAATCCCGTCTACTTCGTCAAACG, AtWNK10 full length; GAGAAGTGTCTTCTCCCAGC/AACTGTGGCTACGTTAAATGA, AtWNK10 front; TTCACCGTGACCTTAAGTGCGACAA/TTGGCGCCATCTACTGCAAGGA.

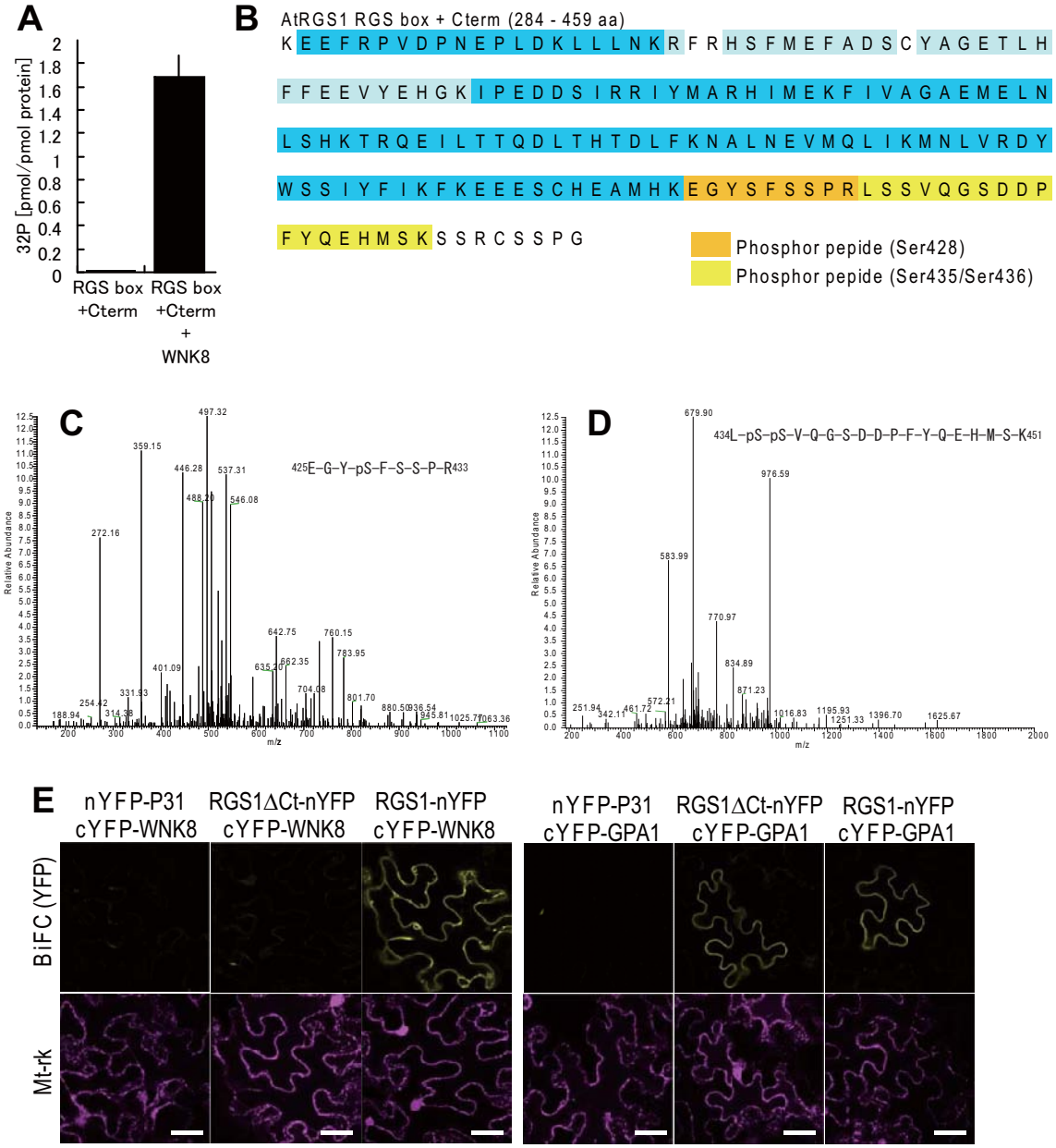

Figure S4 LC-MS/MS spectra of tryptic peptides of RGSbox+Cterm phosphorylated by AtWNK8. (**A**) Stoichiometry of AtRGS1 phosphorylation by AtWNK8. 75 pmol of His-RGSbox+Cterm was incubated with 2.5 pmol of GST-AtWNK8 in 15 μl of buffer containing γ^{32}P-ATP for 8 hr. Proteins were separated on SDS-PAGE and the radioactivity was detected with PHOSPHO image analyzer. Phosphorylation efficiency was calculated with radioactivity of various amounts of standard γ^{32}P-ATP. Data shows mean and SEM from three independent experiments. (**B**) Peptide coverage of the LC/MS/MS analysis. Partial to complete trypsin digestion was used to maximize the coverage of peptides. Residues highlighted were detected. Dark blue highlights detected peptides from complete and partial digestion. Light blue highlights residues detected from partial digestion. Peptides including phosphorylation sites are shown in orange and yellow. Residues not highlighted were not detected. (**C**, **D**) RGSbox+Cterm protein phosphorylated by AtWNK8 was subjected to LC-MS/MS analysis. Peaks corresponding to phosphorylated AtRGS1 peptide are obtained from MS/MS analysis. (**E**) *In vivo* binding between AtRGS1 and AtWNK8. nYFP-tagged AtRGS1, AtRGS1-ΔCt or p31 (negative control) were co-expressed with cYFP-tagged AtWNK8 or AtGPA1 and RFP-tagged Mt-rk in tobacco leaves. Fluorescence complementation of split YFP and expression of RFP were observed by confocal fluorescence microscopy as described in the *Methods*. Scale bars = 50 μm.

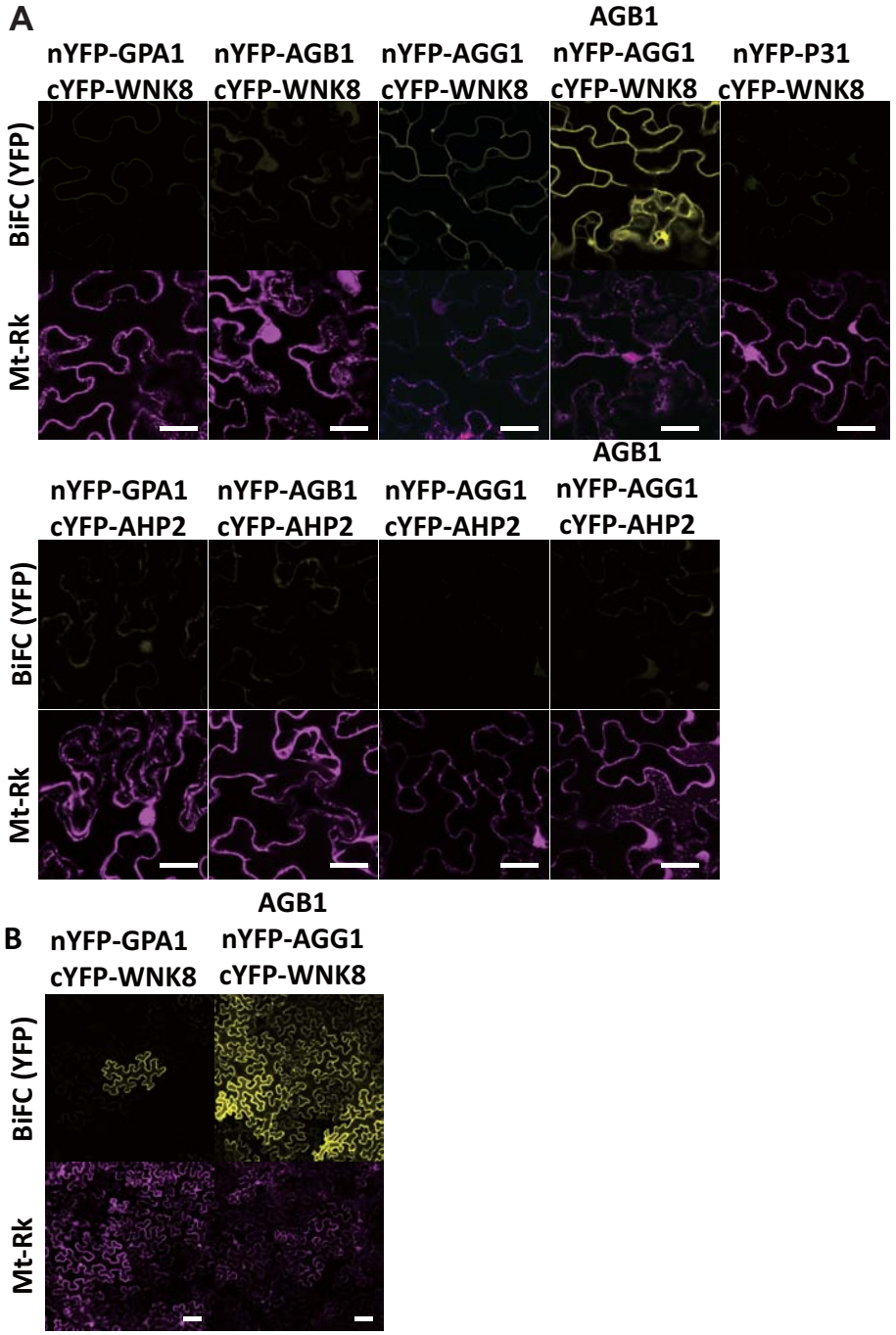

Figure S5 *In vivo* interaction between AtWNK8 and heterotrimeric G-protein subunits. (**A, B**) Tobacco leaves were co-transformed with the indicated nYFP- plus cYFP-tagged proteins (BiFC(YFP)) and a transformation control, RFP-Mt-rk. Fluorescence complementation of split YFP and expression of RFP were observed by a confocal fluorescence microscopy with a 40x objective (A) or a 10x objective lens (B) as described in the Methods. (B) Positive YFP signal was observed occasionally from cells expressing nYFP-AtGPA1 and cYFP-WNK8. Scale bars = 50 μm.

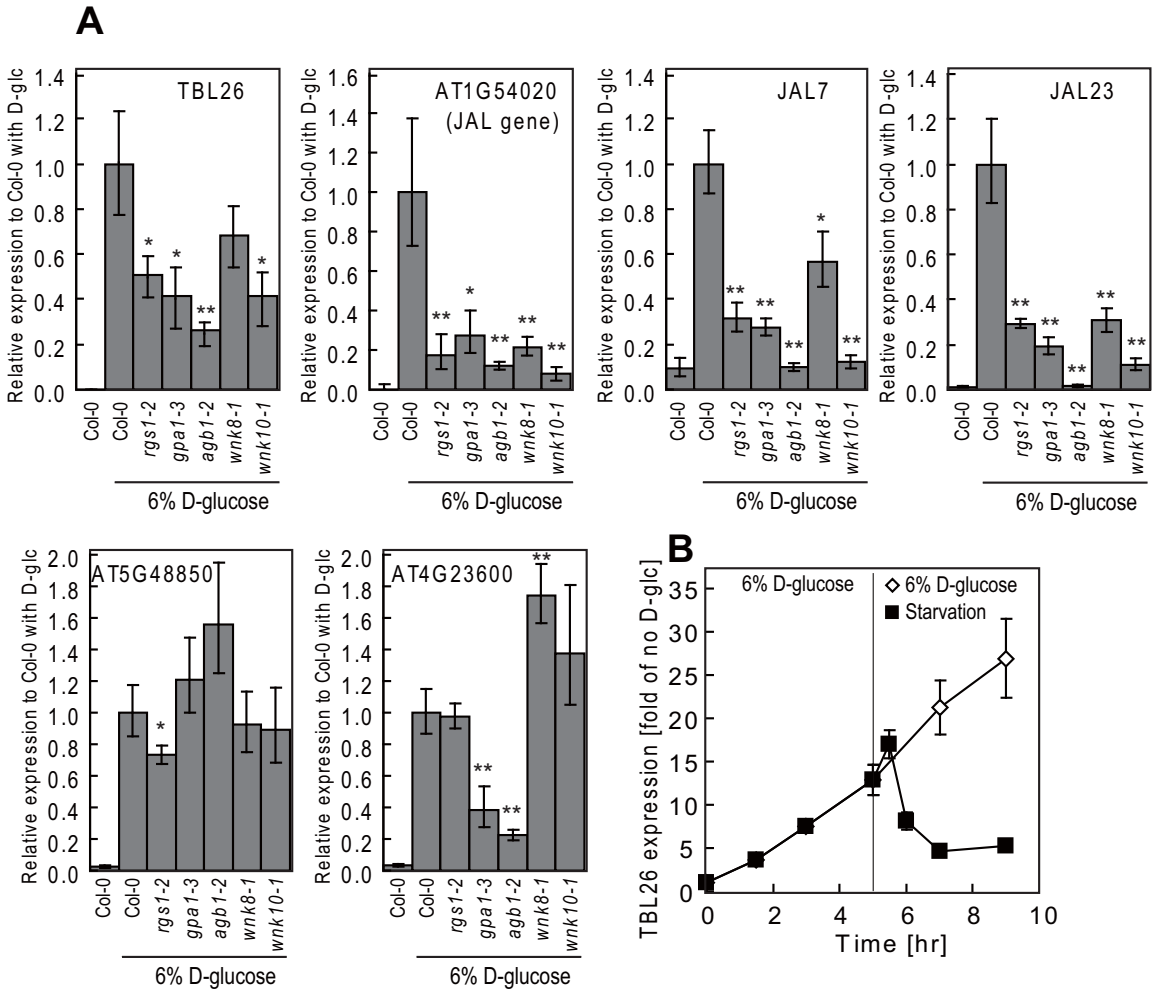

Figure S6 Sugar-reporter gene expression in *wnk mutants*. (**A**) 7-d-old seedlings with the indicated genotypes were starved for 2 days then treated with 6% D-glucose for 3 h as described in ref. 16 with the modifications described in the *Methods*. Transcripts of 6 different sugar-induced genes were analyzed with quantitative PCR. Data are mean ± SD (sample number [n] = 3) from one representative experiment. (**B**) Time course of *TBL26* expression and the reset timing. Wild type seedlings were starved for 2 days and then stimulated with 6% D-glucose for 1, 3, 5, 7, 9 h. After 5 h stimulation, some samples were washed and re-starved in ½ X MS media without sugar for 0.5, 1, 2 and 4 h. *TBL26* expression at each time period was normalized with the expression without D-glucose stimulation. Data are mean ± SD (n = 3) from a representative experiment.

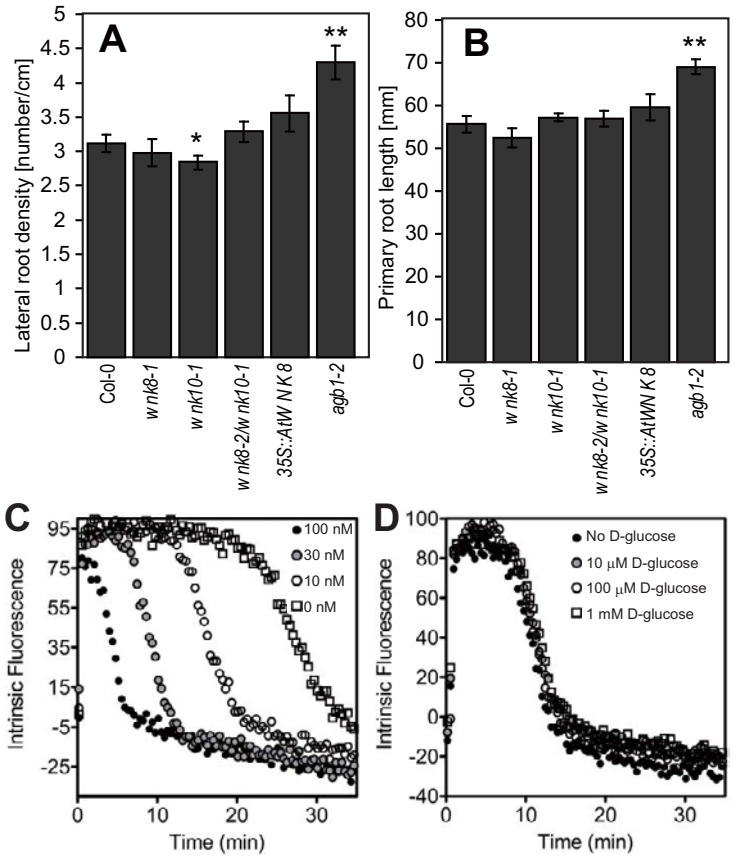

Figure S7 Root phenotype of *wnk* mutants and *in vitro* RGS1 activity (**A**, **B**) Primary root length and lateral root formation of AtWNK-null and AtWNK-expressing plants. Data are calculated from 6 - 11 independent roots from two experiments. (**A**) Seeds from wild type Col-0 and mutant lines sown on ½ X MS plate with 1% sucrose were grown vertically at 23ºC in a short day chamber (8 h light (250 μmol m^{-2} s^{-1}) / 16 h dark). The number of lateral roots were counted on 10-day-old roots. The root number was divided by primary root length. (**B**) Primary root length of 10-d-old roots was measured. Error bars represent SEM. Pairwise Student's *t* test was used to compare values to the Col-0. *, $P < 0.05$; **, $P < 0.01$. *In vitro* GAP activity of AtRGS1 with or without D-glucose. (**C, D**) 400 nM AtGPA1 and indicated concentrations of RGSbox+Cterm were incubated in buffer E (25 mM Tris-HCl (pH 8.0), 1 mM EDTA, 5 mM $MgCl_2$, 100 mM NaCl, and 5% glycerol). 400 nM GTP was added to the cuvette, and the activation and inactivation rates of AtGPA1 were monitored at room temperature by measuring the intrinsic fluorescence of AtGPA1 (excitation at 284 nm, emission at 340 nm) with a Perkin Elmer Luminescence Spectrometer.[7] Data shows a representative result. (**D**) 20 nM RGSbox+Cterm and indicated concentrations of D-glucose were incubated with 400 nM AtGPA1 before adding 400 nM GTP to cuvette. Data shows a representative result from two experiments.

Figure 2C

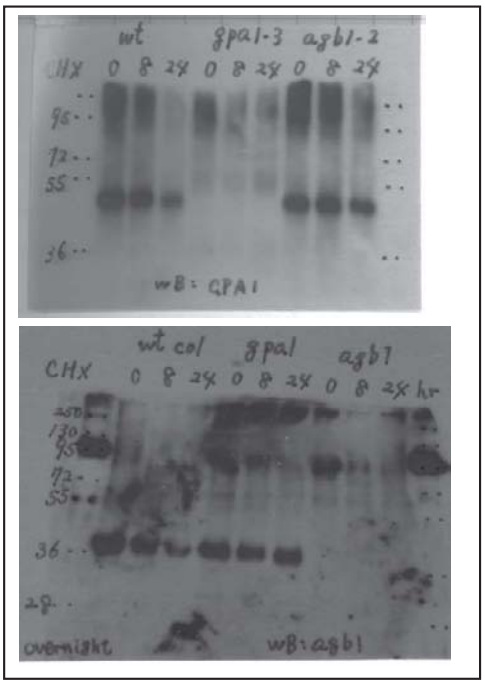

Figure 3A

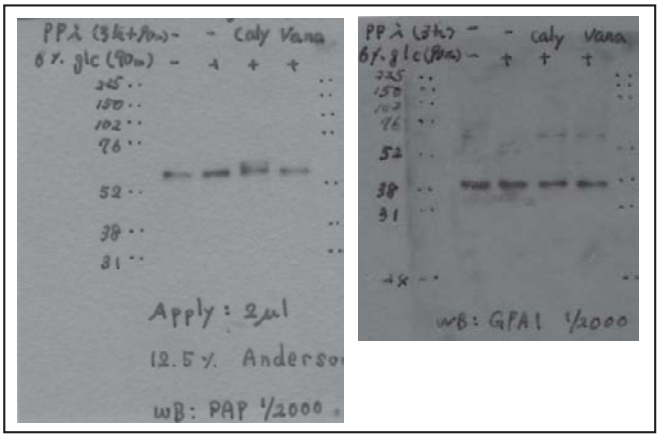

Figure 4C

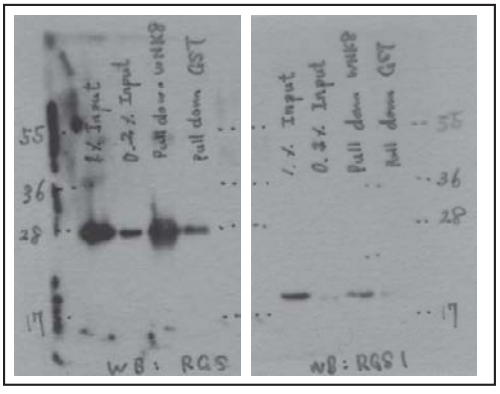

Figure 4G

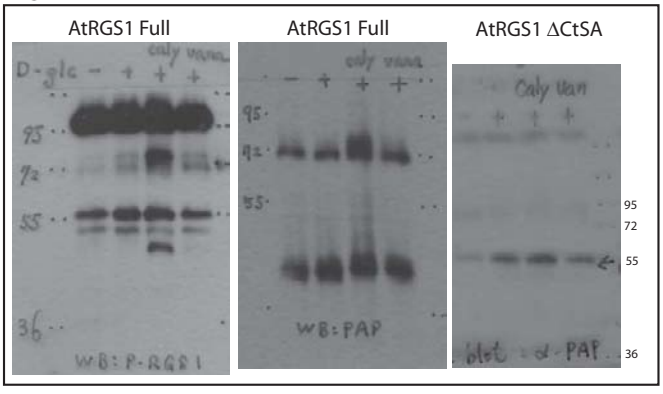

Figure 4F

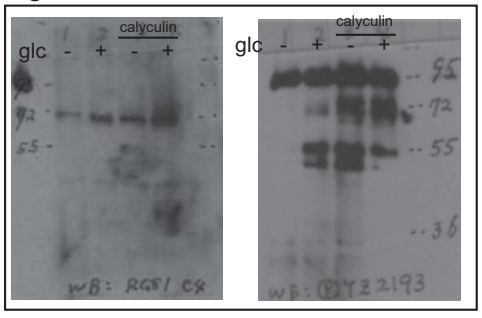

Figure 5A & 5B

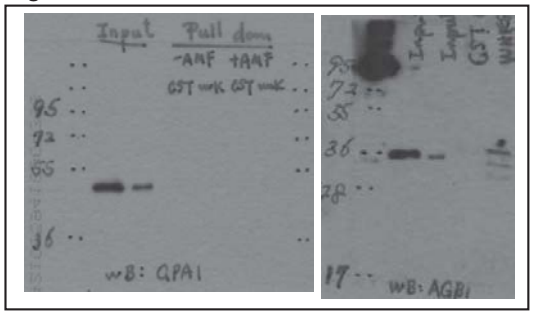

Figure S8 Full scans

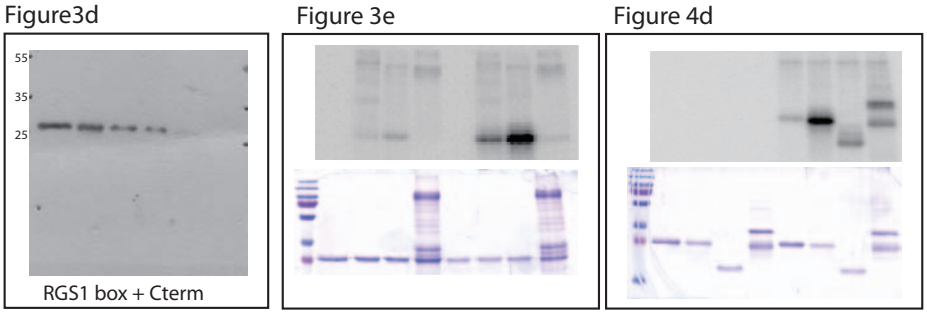

Figure S8 continued